2012•2013
FACULTEIT GENEESKUNDE EN LEVENSWETENSCHAPPEN
master in de biomedische wetenschappen: bio-elektronica en nanotechnologie

Masterproef

Investigating the applicability of heat-transfer resistance as read-out strategy for the detection of mutations in DNA sequences and the detection of neurotransmitters when bound into molecular imprinted polymers

Promotor :
dr. Bart VAN GRINSVEN

Bram Geerets

Masterproef voorgedragen tot het bekomen van de graad van master in de biomedische wetenschappen , afstudeerrichting bio-elektronica en nanotechnologie

2012•2013
FACULTEIT GENEESKUNDE EN LEVENSWETENSCHAPPEN
master in de biomedische wetenschappen: bio-elektronica en nanotechnologie

Masterproef

Investigating the applicability of heat-transfer resistance as read-out strategy for the detection of mutations in DNA sequences and the detection of neurotransmitters when bound into molecular imprinted polymers

Promotor :
dr. Bart VAN GRINSVEN

Bram Geerets
Masterproef voorgedragen tot het bekomen van de graad van master in de biomedische wetenschappen , afstudeerrichting bio-elektronica en nanotechnologie

universiteit hasselt | Maastricht University

Preface

It was October 2010, I was participating in the 4th bachelor year of Medical technology at Zuyd University in Heerlen, when we were instructed to go to a lecture of a professor from Belgium. He was going to give a presentation about surface chemistry. At this point I did not have a clue what we were going to do with this information and I certainly did not have the slightest idea about the effects this acquaintance would have on my further career. After attending the lecture, I spoke to the professor who informed me about the possibility to perform my bachelor thesis writing at Hasselt University. After taking this suggestion into consideration, I decided to make an appointment at this university to discuss possible subjects to obtain my bachelor degree. Here I met a PhD student, Bart, who was performing DNA analysis measurements based on impedance spectroscopy. His enthusiasm for doing this kind of research was sincerely and contagiously and it was due to him that I was persuaded in writing my bachelor thesis in this subject. After performing different types of DNA analysis methods, discovering a new read-out strategy, and having a lot of fun I was able to finish my bachelor thesis with success. By then I had already decided that I wanted to continue this kind of research. I was proud to be admitted to the master Bioelectronics and Nanotechnology at Hasselt University. This was a two year master course combining physics, chemistry and biology. The first lecture I was blown away by the speed at which we were going through this subject. I remember my parents asking me about this first day and I honestly had to say that the matter that we discussed during a five week period during my bachelor degree was treated here in only two hours… This occurred to be the pace during the entire course and with a lot of effort I was able to succeed all theoretical and practical lessons. The final part of the master was a senior practical training and writing a thesis about the subject. I chose to return to the place where I wrote my bachelor thesis and under the supervision of my old mentor I started with my master project. This project was going to be about optimizing the previously discovered heat-transfer method. With great interest I started working at this topic and during this internship I was involved in more and more different studies. It was thanks to one of these studies that I had the opportunity to write my own article. Now at the end of my senior practical training I have achieved to collaborate in three scientific articles (1 first author and 2 co-authors) and I am proud to have been one of the team.

Acknowledgements

Before starting the formal part of this thesis I would like to thank the people who helped, supported, took care and believed in me.

Dr. Bart van Grinsven. From the first time we met during my bachelor internship at IMO you have supported me in a most fun manner. I was able to discover an entire new research world and due to your enthusiastic approach to science you convinced me to start the master in bioelectronics and nanotechnology. During my senior practical training fortunately you were my promoter and mentor, but most of all, now at the end of this internship, I think I can see you as a friend!

Dr. Marloes Peeters. Performing measurements on your account was not hard at all, even though it was about 300 hours of measuring time. You have learned me that you can achieve things much more easily when you are open to it and that having fun in the work that you are doing is the most important part. Most of all I want to thank you for involving me in writing an article. You gave me the opportunity to submit my first scientific article.

Dr. Patricia Losada-Perez and Drs. Andreas Gaulke. Pati thank you for the discussions we had about thermal resistance measurement and you taught me to have a critical view on the results of our accomplished data. But most of all thank you for educating me in the 'scientific' Spanish language. Andreas you were a most welcome guest at the end of my thesis writing. You are a real pro in Word and the appearance of my thesis would have been much less without your efforts!

Mom, Dad. Being the oldest one at home for me meant that I had to discover everything for myself and I think that during this period I have not always been easy to handle.. Mom, Dad I think you taught me a lot, but the most important was to act normal and do the thing you enjoy. Life is already too short so we better live it to the fullest. I think that I surprised you guys when I told that I was entering the master course in Belgium. Nevertheless, you supported me during these 2 years of extreme hard studying and ensured me that everything was going to be alright when I had one of many nervous breakdowns.

Marit, Fieke. As my little sisters I hope I have guided you through child hood with a lot of fun and of course many struggles. I educated the both of you in the alcoholic night outs and trained you to never lose a drinking bet.

Sif. We met in a bar celebrating the exclaim of prince carnival at the day before I had to start my bachelor internship at IMO. Since then our lives are intertwined you had to endure with this poor student while you were already participating in the real world. During the two and a half year of suffering you took care of me by filling my tummy with delicious food and listening to my complaining when things did not work out as I had planned. Hopefully from this moment on I am able to support you as you did supported me. Thank you for persevere all this time with me ☺

Table of Contents

Abstract

The development of biosensing platforms that employ label-free real-time read-out strategies is the topic of interest at this very moment. In the past a sensor platform based on molecular imprinted polymers (MIPs) was developed that utilizes impedance spectroscopy as a read-out strategy. This very same method was also used to detect single nucleotide polymorphisms by chemically denaturing DNA fragments. Recently, a novel read-out format was developed based on the changes in the thermal resistivity of the sensor platform during thermal denaturation of DNA. This so-called heat-transfer method (HTM) enabled the detection of SNPs without the need for mathematical fittings of the data as in impedance based read-out strategies.

In this work, the applicability of HTM as a novel approach for the detection of small molecules on a MIP sensor surface. For proof of principle purposes, three different imprinted sensor surfaces were engaged using L-nicotine, histamine and serotonin as template molecules. For the applying HTM as a read-out strategy, the detection limits of the sensor are acquired to be in the physiologically relevant concentration regime. HTM has proven to detect concentration in the nanomolar range. This concentration range is comparable with the detection limit of a state of the art technique like impedance spectroscopy. The obtained results state it is possible to employ HTM not solely for SNP detection, but it is well applicable for detecting the capturing of small molecules in nanocavities of a polymer layer.

The second part of this thesis was about implementing HTM on a SNP detection array. This was a sequel of the thermal denaturation of DNA research. The sensitivity of HTM was further examined by introducing compartments of complementary and mutated DNA fragments on the same nanocrystalline diamond surface at different ratios of (3:1, 2:2 and 1:3). HTM was engaged to monitor the denaturation process of both types of DNA fragment. This resulted in an applicability of HTM for quantifying DNA fragments of interest, detecting and quantifying SNPs in a mixture of mutated and non-mutated DNA fragments.

The final part focusses on the optimization of the sensor platform. The temperature of the setup is regulated using a proportional integral derivative (PID) controller. The current PID configurations of HTM were evaluated. It was noticed that the origin of the noise was from the power supply. The tuning of PID settings was done in a temperature range, between 35 – 85 °C and we differentiated between plateau phases and ramping phases. The optimal PID parameters appeared to be P1-I6-D0. These settings were employed to study the detection of L-nicotine in buffer solutions, as in chapter 2. The PID tuning resulted in an improvement of the detection limit from 100 nM to 35 nM which is a decrease in noise of nearly a factor of three.

This project has led to the development of a multi applicable read-out strategy based on HTM to detect the capturing of small molecules using MIPs and to monitor the thermal denaturation of different DNA sequences at once. Finally the detection limit of the MIP sensor platform was optimized by enhancing the HTM by tuning the PID configuration.

Nederlandse samenvatting

De ontwikkeling van biosensor platforms, die gebruik maken van label vrije, real-time uitlees strategieën is op dit moment het onderwerp van gesprek. In het verleden zijn er al platforms ontwikkelt die impedantie spectroscopie gebruiken voor het meten van MIPs. Daarnaast werd impedantie spectroscopie ook al gebruikt voor het detecteren van punt mutaties in DNA. Recentelijk is er een nieuw format toegepast dat veranderingen waarneemt in de thermische weerstand van het sensor oppervlak tijdens de denaturatie van DNA. Deze HTM maakte het mogelijk om punt mutaties te detecteren zonder dat het nodig was om mathematische fits van de data te maken, iets wat wel nodig was bij impedantie spectroscopie.

De toepasbaarheid van HTM voor de detectie van kleine moleculen op een MIP sensor oppervlak is in dit werk beschreven. Om dit aan te tonen is er gebruik gemaakt van drie verschillende imprinted sensor oppervlakken voor het detecteren van L-nicotine, histamine en serotonine. Om HTM toe te kunnen passen is het nodig dat de detectie limiet van de sensor in een fysiologisch bereik ligt. Uit de resultaten bleek dat deze techniek het mogelijk maakt om in het nanomolair gebied te meten. Hiermee is aangetoond dat HTM niet alleen voor de detectie van punt mutaties toepasbaar is, maar ook kan worden gebruikt om het aanhechten van kleine moleculen op het sensor oppervlak te detecteren.

Het tweede deel van deze thesis gaat over het toepassen van HTM op een punt mutatie detectie reeks. Dit was een vervolg van het onderzoek naar thermische denaturatie van DNA. De gevoeligheid van HTM is getest geworden door zowel gezond DNA als DNA met mutaties op hetzelfde sensor oppervlak te bevestigen. Hiermee werd het denaturatie proces van beide soorten DNA gelijktijdig gemonitord. Het resultaat hiervan was dat het mogelijk is om onderscheid te maken tussen de verschillende DNA sequenties door het toepassen van HTM.

In het laatste deel beschrijft het optimaliseren van het sensor platform. De temperatuur van de setup wordt geregeld door middel van een PID regelaar. De huidige PID instellingen van HTM werden geëvalueerd. Hieruit kon worden geconcludeerd dat stroomvoorziening de ruis bron is. Het afstellen van de PID regelaar werd gedaan voor een temperatuur bereik tussen 35 – 85 °C en er werd onderscheid gemaakt tussen plateau fases en helling fases. De meest geschikte PID parameters werden bepaald op P1-I6-D0. Deze instellingen werden gebruikt voor het detecteren van L-nicotine in buffer oplossingen, zoals in hoofdstuk 2. Het optimaliseren van de PID configuratie had als gevolg dat de detectie limiet van de sensor verlaagd werd van 100 nM naar 35 nM. Dit is een verlaging met een factor 3.

Dit project heeft tot een multi toepasbare meetmethode waarmee het mogelijk is om zowel kleine moleculen te detecteren als het monitoren van de thermische denaturatie van verschillende DNA sequenties op het zelfde sensor oppervlak. Uiteindelijk is ook het MIP sensor platform geoptimaliseerd door het verbeteren van de HTM door het afstellen van de PID instellingen.

Chapter 1

Introduction

In bioanalytical industry there is an enormous demand for fast, cheap and easy to employ read-out strategies. In this chapter a description is given about various strategies to identify different analytes in solution using molecular imprinted polymers. Furthermore, an insight is given upon analysis and identification methods of DNA sequences. Finally, a brief explanation of the sensor setup of the currently investigated detection method is afforded with an intensive elucidation on proportional – integral – derivative controlling.

1.1 Molecular Imprinted Polymers

Molecular imprinted polymers (MIPs) are based on 'molecular keys' and artificial 'locks'. The polymers are designed to have specific molecular recognition properties, which arise after removal of the template molecule. The imprinted polymer preserves a high affinity to this molecule enabling differentiation with closely related compounds [1]. MIPs have already been proposed as applications for chromatographic stationary phases [2], enantiomeric separations [3], and solid-phase extraction. More recently, MIPs have been used as drug delivery systems and as biosensor [4]. There are several techniques to detect the binding of a template molecule to the MIP layer. Gravimetric detection using quartz crystal microbalances (QCM), or electrochemical sensors are individual techniques capable of analyzing these binding characteristics. The principal of these techniques is detailed below.

1.2 Gravimetric detection

Solid state sensors are appropriate for mass sensing. Their response is based on the electrical interaction of the surface and the implemented molecules. However, these sensors have the inability to differentiate between molecules with the equivalent electrochemical reaction to the surface. In gravimetric detection techniques, like QCM, an electrical potential is directed across the crystal resulting in a vibration with a characteristic frequency. On top of the crystal a functionalized polymer layer is deposited. Attachment of the molecule to the chemical layer will result in an alternation of the resonant frequency of the crystal as depicted in Figure 1. The resonator transduces this shift into an electrical signal by piezoelectric effect. The electrochemical transduction of the frequency response to resonator response enables not only the detection of mass loading, but also can be related to the concentration of the molecule that is introduced. After amplifying and phase-shifting the signal to satisfy the self-oscillating conditions, the signal is re-injected, *via* a closed loped system, in the resonator using a actuation force of piezoelectric origin [5, 6].

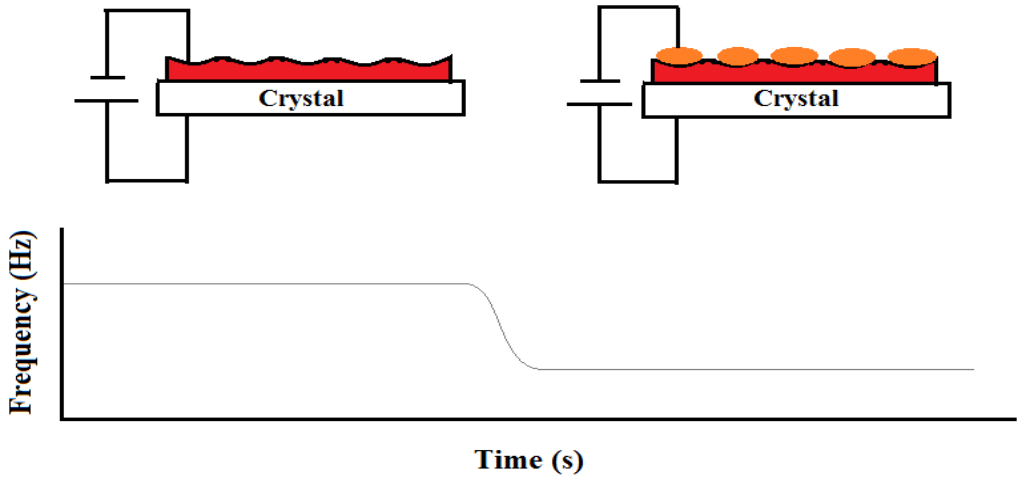

Figure 1: The QCM device registers mass loading on the crystal surface by an alternation of oscillating frequency of the crystal. The presence of template molecules is detected by comparing this frequency before and upon addition of the target molecule.

1.3 Electrochemical biosensing techniques

The principle of a biosensor can be used for implementing electrochemical techniques for MIPs detection. A biosensor consist of a transducer and a biological marker (e.g. enzyme, antibody), which can be replaced by an artificial coat (e.g. MIPs layer). There are different electrochemical techniques which can be performed as read-out strategy.

1.3.1 Conductometric measurements

In the early MIP-based chemical sensors, a conductometric setup was employed containing a MIP is coated onto the membrane among two platinum electrodes which is placed into the analyte. By applying an alternating current, the resistivity of the membrane is defined. Once the analyte contains the specific template this will impose a change in the membrane resistivity. There were two different setups proposed as illustrated in Figure 2; Mosbach *et al.* intended to develop a conductometric setup constructed with an imprinted probe, while Piletsky *et al.* suggested a setup placing the electrodes in two separated containers filled with buffer solution interconnected by the MIP membrane. For both advised setups some difficulties encountered, the first setup has a time elapse of several hours, whereas the second setup struggles upon selecting the membrane [7, 8].

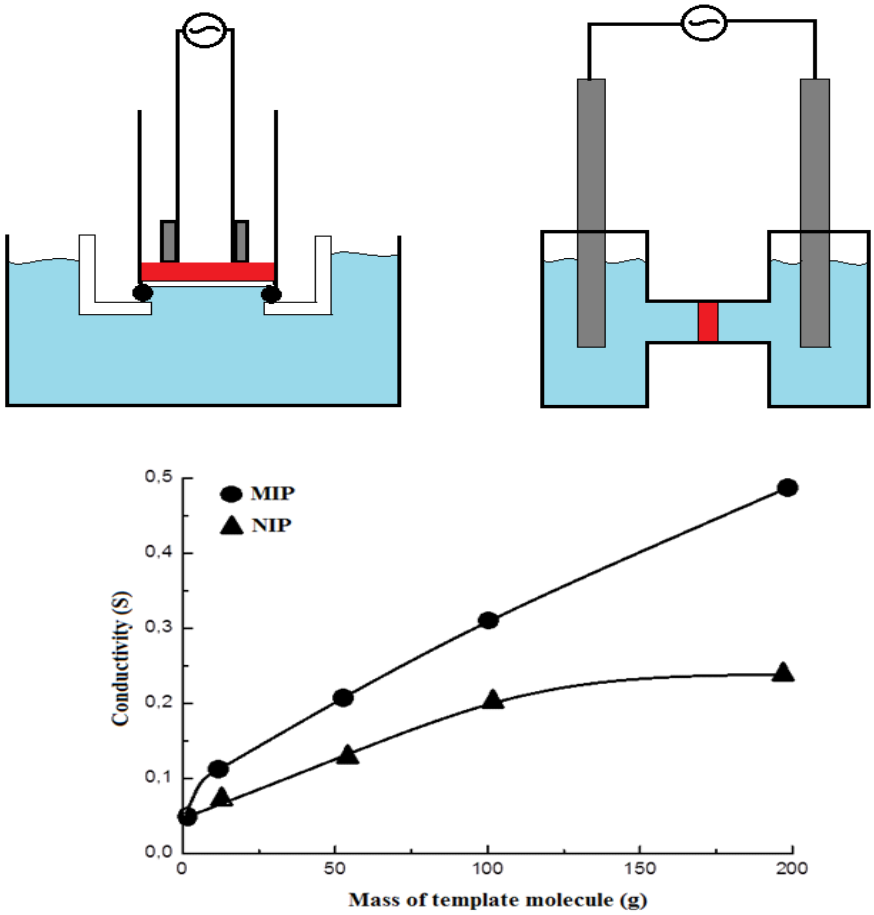

Figure 2: The upper part represents a schematic layout of two conductometric measurement setups. The first setup is proposed by Mosbach *et al.* and measures the conductance of a MIP layer between two platinum electrodes. The second setup is suggested by Piletsky *et al.* and employs two connected containers filled up with solution. Between these containers a MIP based membrane is applied. The graph illustrates the conductivity of the polymer layer in the Mosbach *et al.* setup.

1.3.2 Voltammetric detection methods

There are several detection methods which are grounded from voltammetry. These can be classified on electroactivity of the analyte. The MIP detection can be performed by various read-out techniques, like chronoamperometry, or differential pulse voltammetry (DPV) for electroactive analytes, and DPV, linear scan voltammetry (LSV), or cyclic voltammetry (CV) for non-electroactive analytes. Chronoamperometric read-out makes use of a MIP particle coated electrode and starts with an equilibration of the background electrolyte current. Subsequently, the electroactive analyte is added and it will be attracted by the MIP coated electrode. The current is measured continuously until an equilibrium is reached. The final step is introducing a non electroactive competitor, which will result in releasing the analyte. This will result in a chronoamperometric current peak triggered by accumulation of the released analyte on the electrode which will cause electrochemical oxidation. Besides chronoamperometry also DPV can be employed for electroactive analytes. The MIP electrode is incubated in electroactive analyte. DPV is performed on the accumulated MIP electrode placed in fresh equilibrated electrolyte solution, generating no peaks. At which point a non-electroactive competitor is added. In consequence of this addition, release of the electroactive analyte occur. The gradually release of the analyte causes a rise in current, due to electrochemical interaction with the counter electrode. The principle of the electroactive analyte MIP electrode is demonstrated in Figure 3.

The non-electroactive analytes are investigated using an electroactive competitor (EC). For this purpose three possible methods based on electrochemical transformations are detailed. The first method to describe employs a suspension of MIP particles in non-electroactive analyte incubated with an EC. After a period of binding time, the suspension is centrifuged to remove the MIP particles leaving the unbound analyte and competitor in the solution. DPV or LSV is applied to detect the unbound EC. Another approach suggests to use a MIP coated electrode and incubate in a solution of non-active analyte and EC. Hence, replace the solution by fresh electrolyte solution and utilize DPV to measure the bound EC on the electrode. For the third method, a thin layer of MIP is coated on the electrode. CV was engaged to measure the electric activity of an electroactive indicator in the absence of the template. Subsequently, the analyte containing the template is introduced to the solution, resulting an improved diffusion permeability of the MIP layer due to the presence of the template when CV is executed. This is reported as ‘gate effect’ [9, 10].

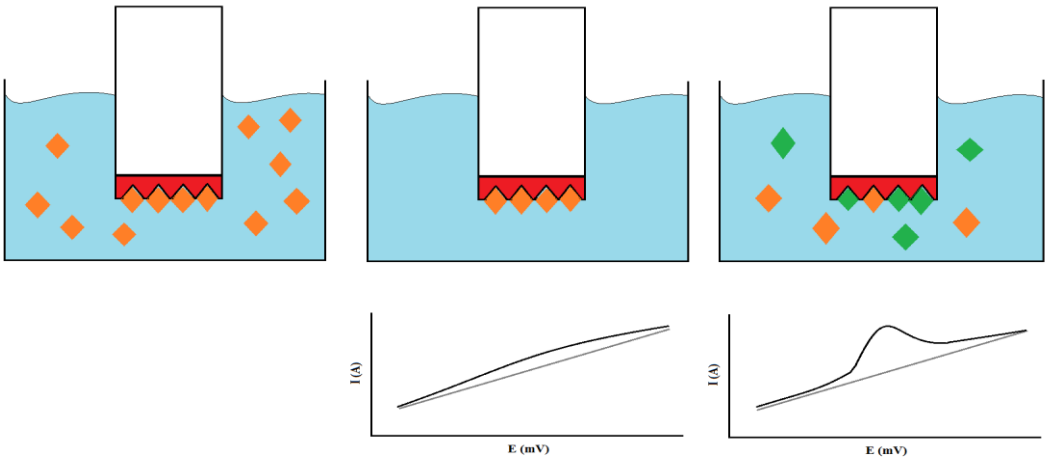

Figure 3: The upper figure presents the binding of an electroactive analyte to the MIP coated electrode. After binding the electrode is placed in a fresh electrolyte, something striking appears when adding a non-electroactive competitor to the analyte. The released electroactive analyte causes a peak in the IV-curve.

1.3.3 Potentiometric sensing

Ion selective electrodes are employed for potentiometric read-out. Compared to other electrochemical read-out techniques, the template molecules do not have to diffuse through a membrane making the measurement less time-consuming. For MIP based potentiometric detection, the polymer is imprinted with the ion of interest by preparing the polymer in an electrolyte which contains the ion of interest. Figure 4 gives a schematic view of the sensor setup. After removal of the MIP out of the electrolyte, the layer memorizes the ion, keeping the affinity for this particular ion. The anion is attracted into the imprinted area resulting in an electrochemical reaction which is monitored *via* the potentiometric transducer providing an electrical signal [11].

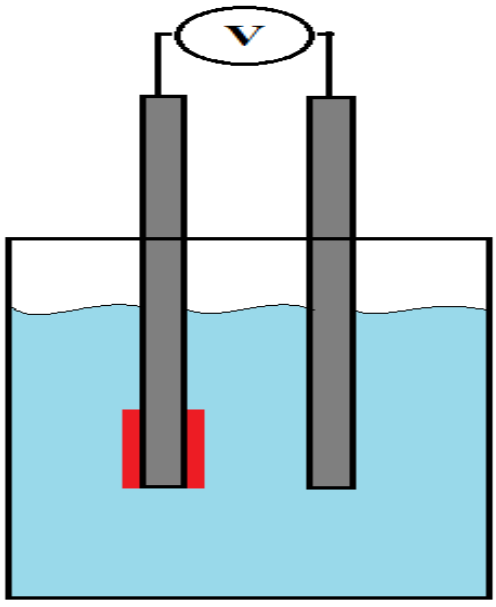

Figure 4: The potential is measured using two platinum electrode. One electrode is coated with a polymer prepared in an electrolyte containing the ion of interest, resulting in a change in potential when the anions anneal to the electrode surface.

1.3.4 Impedance spectroscopy

Over the last decade, intensive research has been performed in the development of label-free biosensors [12-15]. Hereby, ensuring the absence of the need for fluorescent labeling techniques, and expensive optical read-out equipment. Such label-free read-out technique was proven to be impedance spectroscopy [16, 17]. Impedance spectroscopy was already used in the development of novel medical equipment for the detection of neurotransmitters, proteins, or point mutations in DNA. For example, it was used for the electronic detection of serotonin in human blood plasma using MIPs [18], the electronic read-out of an immunosensor for C-reactive protein (CRP) [19, 20], and the real-time monitoring of the chemical denaturation of DNA (Figure 5) [21]. Moreover, impedance spectroscopy was also utilized in the food industry to detect mycotoxins [22], or to determine the salt content in food products [23].

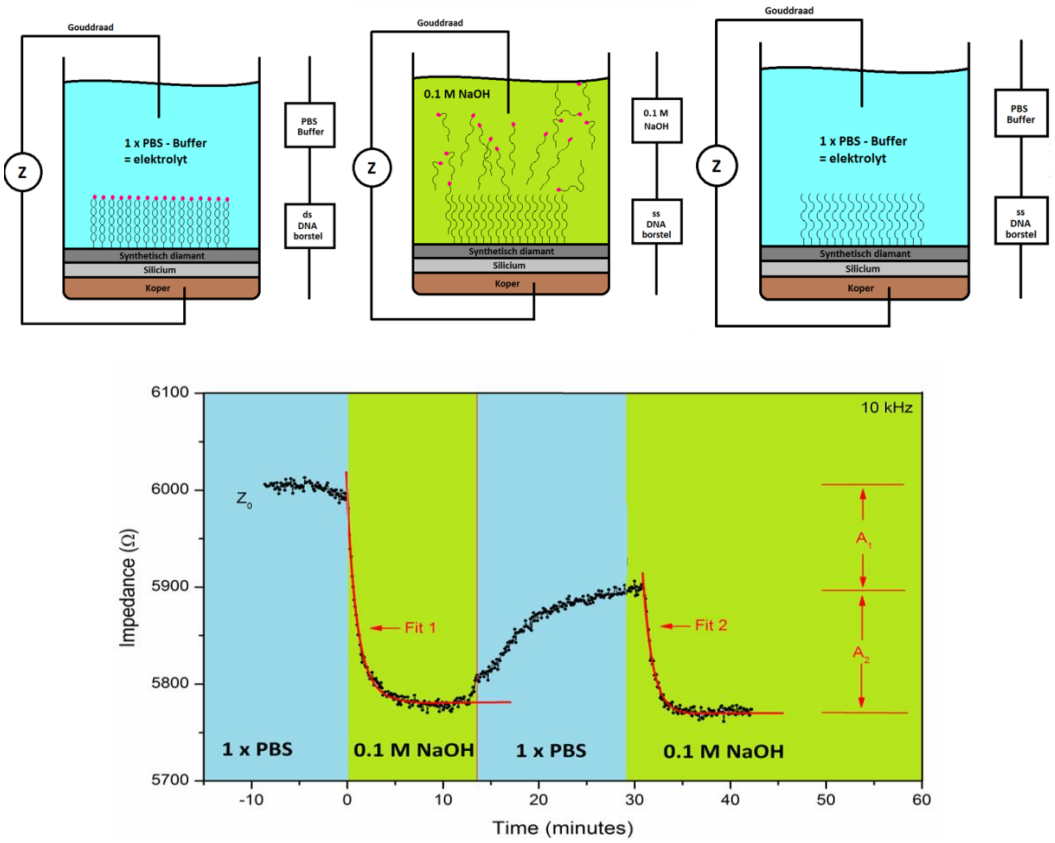

Figure 5: The chemical denaturation of DNA is monitored by impedance spectroscopy. DNA denatures by addition of NaOH. In the graph, a drop in impedance is noticed when the PBS medium is substituted by NaOH. This is the effect of denaturing the DNA and changing the medium. Therefore, PBS is injected once more resulting in an increase in impedance. Finally, the PBS is substituted again by NaOH. However this time the effect in impedance is caused only by medium exchange.

In impedance spectroscopy a small alternating voltage is applied varying in frequency in a predefined regime. The impedance is measured between the working electrode (MIPs layer on aluminum substrate) and the counter electrode in the liquid. The impedance alters when template molecules are captured on the working electrode enabling the specific detection.

The impedimetric data can be represented by a Nyquist or a Bode plot. In the higher frequencies the Nyquist plot shows a semicircle region followed by a linear behaviour in the lower frequency range. This specific

representation corresponds to the charge-transfer process that occurs in the higher frequency range, while the activities of the lower frequency regime illustrates the diffusion controlled process. However, in spite of the advantages of impedance spectroscopy for practicing in label-free measurements there are certain drawbacks. To obtain the end results first a number of calculations and fittings have to be performed, which is inconvenient when implementing impedance spectroscopy in a medical laboratory environment.

1.4 DNA

That the hereditary information is carried on chromosomes was already discovered in the late 19th century. However, it was not until the 1940s DNA was identified as the carrier of genetic information. Moreover, the mystery of how proteins could be specified by instructions in the DNA was not yet to be solved until 1953. When James Watson and Francis Crick made their famous predicting about the structure of DNA. Their work is a cornerstone in the history of biochemistry. In order to forecast there assumptions, they enforced x-ray diffraction analysis obtained from x-ray diffraction photographs acquired by Rosalind Franklin, Raymond Gosling and Maurice Wilkins. By combining this information with Chargaff's rule, who stated that, respectively, *Adenine and Thymine*, and *Cytosine and Guanine* are present in equimolar quantities, Watson and Crick concluded that DNA is composed of two strands of the polymer entwined around each other in a double helical structure [24, 25]. As can be seen in Figure 6.

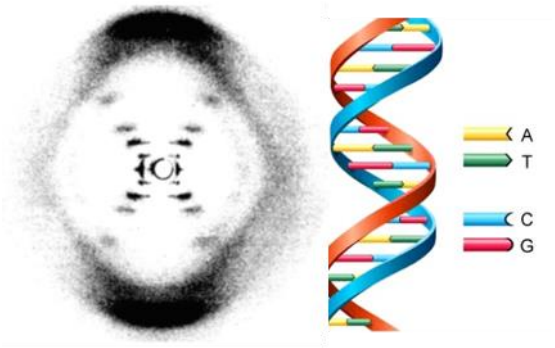

Figure 6: The x-ray diffraction image originated by Rosalind Franklin, Raymond Gosling and Maurice Wilkins is depicted on the left side of the figure. On the right side the double helical structure of DNA is shown. In here, the complementary base pairs are visualized on the interior of the structure. While the sugar-phosphate backbone is shown on the exterior of the structure.

A deoxyribonucleic acid (DNA) molecule consists of two long polynucleotide chains. However, the composition of these chains exist only out of four different types of nucleotides, adenine (A), cytosine (C), guanine (G), and thymine (T). These nucleotides form the base of the strand. The backbone comprehends alternating sugar-phosphate-sugar-phosphate groups. It appears to be that a bulkier two-ring base always is paired with a single-ring base. Hydrogen bonds are constructed between the bases of the different strands, respectively, a double hydrogen bond when A pairs with T (A=T), and a triple hydrogen bond when C pairs with G (C≡G). These are called the complementary base pairs following Chargaff's rule. This is visualized in Figure 7. Hereby, the DNA strands are packed in their most favourable energetic arrangement [25, 26].

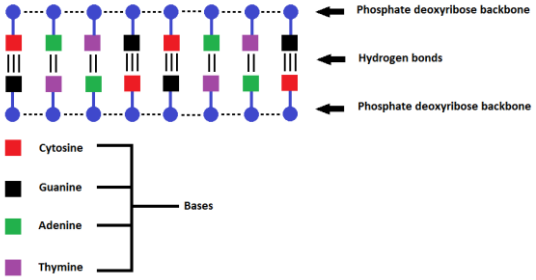

Figure 7: The complementary base pairs predicted by Chargaff's rule. In here , A pairs with T and C forms a couple with G. This pairing occurs by forming hydrogen bonds, respectively, 2 bonds for A-T and 3 bonds for C-G pairs.

1.5 DNA analysis

Various types of diseases encounter due to the presence of pathogenic mutations in the human genome. Well known examples are breast cancer, sickle cell anaemia or Duchenne muscular dystrophies. Therefore, the development of mutation detection techniques is a topic of interest. At this very moment there are several techniques capable of detecting these mutations in a DNA sequence. The most common methods for analyzing DNA sequences are either based on hybridization or denaturation of DNA strands. In the next paragraphs, a selection of genetic analysis tools are discussed.

1.5.1 Microarrays

Microarrays are applied for various analysis, e.g. proteins, cells, or DNA. For DNA there are multiple techniques which employ microarrays. However, the basics are the same for each technique. A solid surface is chemically functionalized by arraying a series of oligonucleotides. The oligonucleotides are used as the identifier by hybridizing an unknown sequence to the probe DNA. There are three different formats for DNA microarrays. Firstly, there are hybridization arrays. Here, the target sequence, tethered with a fluorescent molecule, is hybridized with different series of probe DNA. The number of complementary base pairs determines the strength of the double stranded DNA sequence. A washing procedure is used to remove the non-complementary strands leaving only DNA sequences containing the fluorescent marker, as can be seen in Figure 8. Secondly, electric field microarrays are applied to direct the oligonucleotides to the surface eliminating the need for chemical binding of the probe DNA. The support comprises of a modified agarose matrix. Furthermore, the hybridization of the target DNA is supported by applying electric fields ensuring a tremendous decrease in the duration of hybridization and washing procedures. Thirdly, arrayed primer extension is an employed format. Oligonucleotides are arrayed to a solid support surface. Subsequently, polymer chain reaction (PCR) products are hybridized to the probes, DNA polymerase with four differently fluorescently labeled dideoxynucleotides is applied for each arrayed oligonucleotide. Here, the oligonucleotides act as primer. The fluorescently labeled nucleotides end the PCR reaction rendering the DNA sequence of the target DNA [27, 28].

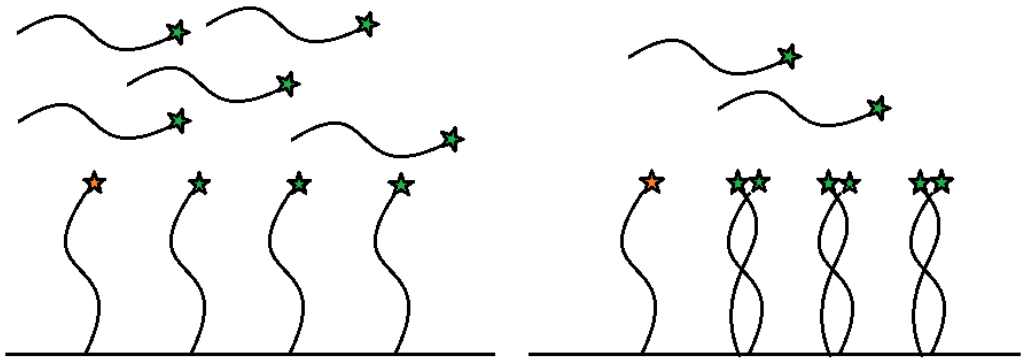

Figure 8: The microarray identifies the hybridization of DNA. The surface contains of different composition of single stranded DNA fragments. The strength of the binding of target DNA is determined by the number of matching sequences. After a washing step only the DNA strands with a high number of matching base pairs remain at the surface. In here illustrated by the green star fragments.

1.5.2 Gel electrophoresis

There are two gel based electrophoresis formats to define the melting domains of a DNA sequence. The first technique to discuss is predicated upon denaturation-gradient, while the second technique is founded on temperature-gradient. However, both methods rely on the negatively charged DNA strand which is attracted through the pores of a gel towards the positive electrode by applying an electric force. In denaturation-gradient gel electrophoresis (DGGE) a constant temperature is administered while the presence of denaturing chemicals in the gel is enhanced causing the DNA to unwind. A schematic representation of DGGE is given in Figure 9. For the temperature-gradient gel electrophoresis (TGGE) an accession in temperature of the gel is noticed towards the positive electrode. The DNA strand has a specific melting point which results in unwinding the DNA strand at this exact position in the gel. For both techniques applies the unwinding of DNA causes a dramatically decrease in movement through the gel. Hereby, it is possible to identify differences in DNA sequences caused by single base pair substitutions, insertions or deletions [29].

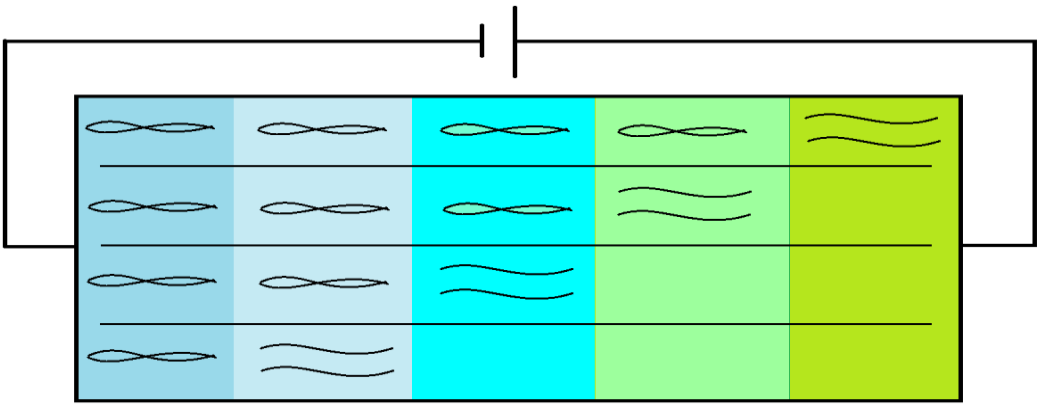

Figure 9: DGGE employs a direct current to attract double stranded DNA fragments through a gel with increasing concentrations of denaturation chemicals. The distance that is covered depends on the completeness of the DNA sequence. A sequence with multiple mismatches denatures at a lower concentration of chemicals compared to a full match sequence.

1.5.3 Heat-transfer method

In 2011, Van Grinsven *et al* reported on thermal denaturation of double stranded DNA by examining the heat-transfer dependent properties. This study provided evidence for thermally denaturing DNA without the use of electrochemical techniques. In comparison with the chemical denaturation of DNA employing impedance spectroscopy as read-out technique, there is no need for medium exchange, neither it is necessary to fit the results with exponential decay curves. The outcome of this study implied that double stranded DNA has a lower thermal resistivity at the solid-liquid interface compared to single stranded DNA. The implemented thermal denaturation occurred to be a fast, label-free detection technique even for discriminating between mismatch DNA strands containing only one single nucleotide polymorphism in the sequence. The principle of heat-transfer method is founded on the transduction of heat by the sensor surface and is measureable by utilizing the temperature difference between two thermocouples and the applied power needed for the heat source. Thermally denaturing DNA resulted in an anomaly in this heat transduction detected by the second thermocouple. The anomaly occurs due to a higher surface coverage of the sensor surface. Double stranded DNA is illustrated as a 'stiff rot', which curls up after denaturing due to the deficiency of stability in this state (Figure 10). Hereby, providing the explanatory for the increase in thermal resistivity [30].

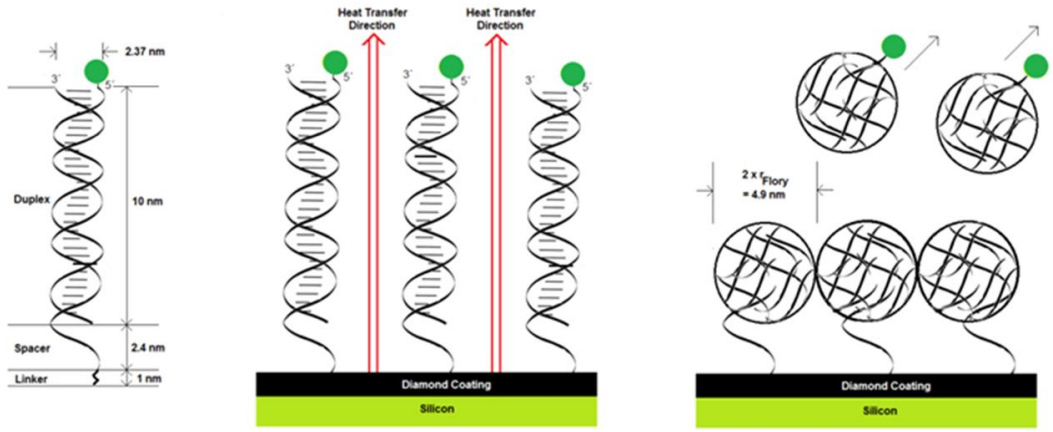

Figure 10: DNA in a double stranded state with a persistence length of 29-mers acts like a stiff rod. Heat travels easily through the DNA fragments standing in this position. Thermal denaturing induces the removal of target DNA leaving only a single stranded fragment. The probe DNA bares insufficient stability to keep the standing position and tumbles over each other. This results in an increase in the thermal resistivity of the sensor platform.

1.6 Sensor setup

A home-made sensor setup was developed to employ HTM measurements. The components of the setup are detailed in [30]. However, the important accessories are described for a further understanding of the setup. The HTM flow cell consists of a three important features, a copper lid, thermocouples, and a Perspex flow cell. Figure 11 depicts a schematically representation of the mounted sensor cell. The sensor surface is attached between the flow cell and the copper lid. The copper is heated utilizing a power resistor and the exact temperature is registered *via* a thermocouple placed inside the lid. A second thermocouple is positioned in the flow cell recording the temperature of the liquid. The bottom of the flow cell comprises a quarts glass enabling possible microscopic read-out. The heat-transfer related parameters are the temperature difference $T_1 - T_2$ and the input power P provided by the heating element. The control of the heating element is intensively described below.

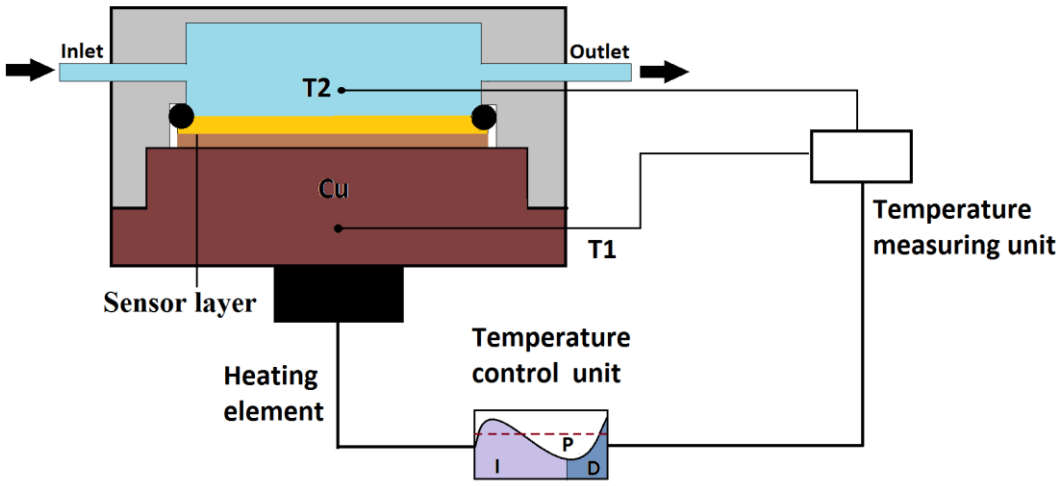

Figure 11: A schematic representation of the sensor platform is illustrated. The setup comprises a heating element attached to a copper lid. The sensor surface is annealed to the copper and screwed on top of the flow cell. The temperature of the copper and the medium are registered and monitored using two thermocouples and the temperature of the copper lid is controlled using a PID controller.

1.6.1 The control system

The sensor setup contains a temperature control unit embracing a feedback system to monitor and control the copper temperature. The feedback system is characterized as a closed loop system, system 1 corresponds to the temperature control unit and system 2 represents the thermocouple responsible for the registration of the copper temperature. The feedback of system 2 influences the action of the temperature controller directly. The closed loop feedback system is presented in Figure 12 The described feedback system also is present in a biological environment. For example, the regulation of glucose level in the human body is arranged by the liver and the pancreas. The liver releases glucose in the blood. In order to maintain a stable glucose concentration the pancreas reacts to this amount by secretion of glucagon or insulin [31].

To control the copper temperature of the setup, we have combined an algorithm with a feedback loop. This algorithm functions as a set point controller as used in a thermostat. The device measures and compares the temperature with the predefined set point. The error between these values determines the action to be taken by the heating plant. In our setup a proportional integral derivative (PID) controller is employed to regulate the

engaged power for heating the system. In modern industry PID systems are also implemented in hydraulic [32], hydro power [33], electric power [34] systems. The controller implements the proportional value as the present error, where the integral and derivative correspond to the average of the past errors and the prediction of future errors respectively and determine the control action, as can be seen in Figure 12. Originally this type of controller is stated as a three-term controller.

$$(1) \quad u(t) = ke(t) + k_i \int_0^t e(\tau)d\tau + k_d \frac{de}{dt}$$

The basic algorithm behind this control unit clearly expresses a sum of the three terms. In here, the control error is represented by e. The control error is determined by the difference between the reference value and the process variable. This reference value is also denominated as the set point. The process variable embodies the current position of the system. The controller parameters are k, k_i, k_d representing the proportional, integral, and derivative gain respectively. In order to decrease the error of the signal, the proportional gain ought to be increased. However, increasing k will conduct to a more oscillating signal [35]. Therefore, proportional gain is only one of the assets to provide an equality between set point and actual temperature. Integral action is the second component to control the temperature. This aspect ensures the output temperature to be equal to the set point when a steady state is accomplished. The integral gain is a measure of the effectiveness disturbance attenuation of the signal. However, a large gain for k_i deteriorates the signal by giving rise to oscillatory behaviour, poor robustness, and possible instability [36]. The aforementioned PID controller is defined as a three-term controller. The third parameter to discuss is derivative action. Increasing k_d guarantees more damping of the signal and hereby reducing the oscillatory effects of previously discussed parameters. However, a too large derivative gain deteriorates the signal tremendously. Therefore, derivative action is recommended for second order dynamics [37].

The parameters of the PID controller can be obtained by numerical or systematic methods. However, in an adaptive control and auto-tuning system these methods are inappropriate. Here, one of the most proper tuning methods are internal model control and gain and phase margin tuning [38]. Nevertheless, for the PID controller used in this setup a systematic approach is suitable to employ.

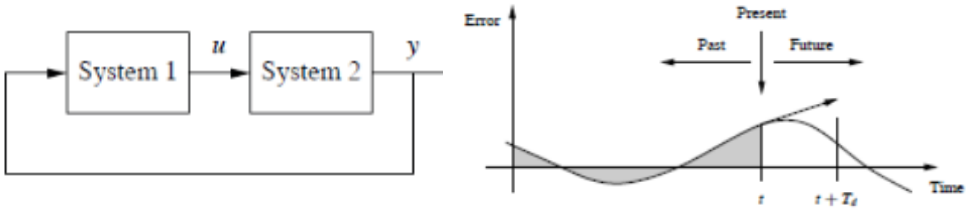

Figure 12: The diagram on the left represents the feedback system. The right graph embodies the tendency of the PID parameters. The proportional value corresponds to the present error, the integral parameter employs the errors of the past, and the derivative setting engages extrapolation to predict future errors.

1.7 Problem statement

In a perfect world, one sensor platform can be employed to perform numerous types of measurements. One type of device to administer SNP detection, to demonstrate the presence of neurotransmitters or small molecules or even the detect living cells. Since 2011 there have been achievements in developing a sensor platform for the detection of SNPs predicated upon HTM which are very promising. This technique registers the change in thermal resistivity of the sensor layer once DNA denatures to its single stranded state. Hereby, a first indication of a fast, label free and easy to implement method was provided. The theory of monitoring changes in surface resistivity is widely applicable, for instance the capturing of template molecules on a MIPs surface should alter the thermal conductance of the layer. This is one of the challenging theoretic to implement in practice. Another challenge is to distinguish between a healthy DNA sequence and a mutated DNA sequence when mounted on the same sensor surface. Van Grinsven *et al.* already proved the ability to differentiate between these two by HTM. However, the measurements were performed separately from each other. In order to employ HTM as a universal format for executing biological measurements the signal – to – noise ratio has to be enhanced. This is the third and final challenge to accomplish. The HTM can be optimized by amending the thermal read-out system by seeking for the optimal PID configuration.

1.8 References

[1] Mayes, A, Whitcombe, M, *Adv. Drug Deliv. Rev.*, 2005, **57**, 1742-1778.

[2] Tamayo, F, Martin-Esteban, A, *J. Chromat. A*, 2005, **1098**, 116-122.

[3] Cheong, W, et al., *Talanta*, 2013, **106**, 45-59.

[4] Piletsky, S, Chianella, I, *Molecularly Imprinted Sensors*, 2012, 339-354.

[5] Jenik, M, et al., *Biosens. and Bioelecs.*, 2009, **25**, 9-14.

[6] Dickert, F, et al., *Sens and Act. B Chem.*, 2001, **76**, 295-298.

[7] Kriz, D, Kempe, M, Mosbach, K, *Sens. and Act. B Chem.*, 1996, **33**, 178-181.

[8] Piletsky, S, et al., *J. Mem. Sci.*, 1999, **157**, 263-278.

[9] Merkoçi, A, Alegret, S, *Trends in Anal. Chem.*, 2002, **21**, 717-725.

[10] Alizadeh, T, et al., *Talanta*, 2009, **79**, 1197-1203.

[11] Tonelli, D, et al., *Electrochimica Acta*, 2011, **56**, 7149-7154.

[12] Lin, B, Li, P, Cunningham, B, *Sens. and Act. B Chem.*, 2006, **114**, 559-564.

[13] Qureshi, A, Gurbuz, Y, Niazi, J, *Proc. Eng.*, 2010, **5**, 828-830.

[14] Schmitt, K, et al., *Biosens Bioelectron*, 2007, **22**, 2591-7.

[15] Wang, J, Kawde, A, *Anal. Chim. Acta*, 2001, **431**, 219-224.

[16] Van Grinsven, B, et al., *Phys. Stat. Sol. A*, 2010, **207**, 919-923.

[17] Vermeeren, V, et al., *Langmuir*, 2007, **23**, 13193-13202.

[18] Peeters, M, et al., *Sens. and Act. B Chem*., 2012, **171-172**, 602-610.

[19] Vermeeren, V, et al., *Sens. and Act. B Chem.*, 2011, **157**, 130-138.

[20] Bryan, T, et al., *Biosens. Bioelectron.*, 2013 **39**, 94-8.

[21] Van Grinsven, B, et al., *Lab on a Chip*, 2011, **11**, 1656-1663.

[22] Zamfir, L, et al., *Sens. and Act. B Chem.*, 2011, **159**, 178-184.

[23] Masot, R, et al., *Sens. and Act. A Phys.*, 2010, **158**, 217-223.

[24] Lucas, A, et al., *J. of Chem. Educ.*, 1999, **76**, 378-383.

[25] Bettelheim, F, et al., *Introduction to General, Organic, and Biochemistry*, 2010.

[26] Alberts, B, et al., *Molecular Biology of the* Cell, 2008.

[27] Karakach, T, et al., *Chem. and Intel. Lab. Systems*, 2010, **104**, 28-52.

[28] Gut, I, *Human Mutation*, 2001, **17**, 474-492.

[29] Lodewyckx, L, et al., *Human Mutation*, 2001, **18**, 243-250.

[30] Van Grinsven, B, et al., *ACS Nano*, 2012, **6**, 2712-2721.

[31] Bouman, L, Bernards, J, Boddeke, H, *Medische Fysiologie*, 2008.

[32] Truong, D, Ahn, K, *Mechatronics*, 2009, **19**, 233-246.

[33] Khodabakhshian, A, Hooshmand, R, *Int. J. Elect Power Energy Syst.*, 2010, **32**, 375-382.

[34] Bevrani, H, Hiyama, T, Bevrani, H, *Int. J. Elect Power Energy Syst.*, 2011, **33**, 179-188.

[35] Shamsuzzoha, M, Skogestad, S, *J. Process Control*, 2010, **20**, 1220-1234.

[36] Åström, K, Murray, R, *Feedback Systems*, 2008.

[37] Skogestad, S, *J. of Process Control*, 2003, **13**, 291-309.

[38] Weng, K, Chang, C, Lisheng S, *Automatica*, 1995, **31**, 497-502

Chapter 2

Heat-transfer based detection of L-nicotine, histamine, and serotonin using molecularly imprinted polymers as biomimetic receptors

Analytical Bioanaytical Chemistry, 2013, (DOI) 10.1007/s00216-013-7024-9

M. Peeters[1], P. Csipai[1,2], **B. Geerets[1]**, A. Weustenraed[1], B. van Grinsven[1], J. Gruber[2], W. De Ceuninck[1,3], T.J. Cleij[1], F.J. Troost[4], P. Wagner[1,3].

1) Institute for Materials Research, Hasselt University, Wetenschapspark 1, 3590 Diepenbeek, Belgium.
2) Universidade de São Paulo, Instituto de Química, Av. Prof. Lineu Prestes, 748 CEP 05508-000 São Paulo, SP, Brazil.
3) IMEC vzw, division IMOMEC, Wetenschapspark 1, 3590 Diepenbeek, Belgium.
4) Department of Internal Medicine, div. of Gastroenterology – Hepatology, Maastricht University Medical Center, Minderbroedersberg 4-6, 6211 LK Maastricht, The Netherlands.

2.1 Abstract

In this work, we will present a novel approach for the detection of small-molecules with Molecularly Imprinted Polymers (MIP)-type receptors. This heat-transfer method (HTM) is based on the change in heat-transfer resistance imposed upon binding of target molecules to the MIP nanocavities. Simultaneously with that technique, the impedance is measured to validate the results. For proof-of-principle purposes, aluminum electrodes are functionalized with MIP particles and L-nicotine measurements are performed in phosphate buffered saline (PBS) solutions. To determine if this could be extended to other templates, histamine and serotonin samples in buffer solutions are also studied. The developed sensor platform is proven to be specific for a variety of target molecules, which is in agreement with impedance spectroscopy reference tests. In addition, detection limits in the nanomolar range could be achieved, which is well within the physiologically relevant concentration regime. These limits are comparable to impedance spectroscopy, which is considered one of the state-of-the-art techniques for the analysis of small molecules with MIPs. As a first demonstration of the applicability in biological samples, measurements are performed on saliva samples spiked with L-nicotine. In summary, the combination of MIPs with HTM as novel read-out technique enables fast and low-cost measurements in buffer solutions with the possibility of extending to biological samples.

2.2 Introduction

Molecularly Imprinted Polymers (MIPs) are synthetic receptors which can bind their target as specific and selective as an enzyme [1, 2]. The focus of the imprinting strategy was originally on small organic molecules, but the technique has been extended to biological molecules such as proteins [3] and living cells [4, 5, 6]. As compared to natural antibodies, the advantages of MIPs are the low-cost and straightforward production [7], unlimited shelf life [8] and good thermal and chemical stability [9]. Depending on the required morphology, the MIP synthesis can be performed with various methods including bulk polymerization [10], emulsion polymerization [11] and electropolymerization [12]. We will focus here on the most commonly used method, which is bulkpolymerization since it is straightforward and widely applicable.

In recent years, the interest from the bio-analyical field has increased rapidly because MIPs are extremely suitable for the detection of chemical targets in complex matrices such as urine, blood and saliva [13]. For separation purposes, MIPs can be readily used by packing them directly into separation columns [14]. The main drawbacks of chromatographic techniques are the often time-consuming measurements and the requirement of expensive equipment [15,16]. The incorporation of MIPs into sensing devices remains therefore challenging. In literature, the majority of the sensor platforms is based on gravimetric detection [17] and electronic read-out platforms [18, 19]. In contrast, electrochemical techniques are inexpensive but the analysis is often complicated. There are a few examples of MIP measurements in biological samples such as in human blood plasma [20], intestinal fluid [21], blood serum [22, 23] and urine [23]. These measurements are all *in vitro*; until now little has been reported about their application in living organisms. Hoshino *et al*. [24] studied the behavior of molecularly imprinted polymer nanoparticles for mellitin *in vivo*. With fluorescent labeling of the target, they could determine that the nanoparticles could effectively capture the mellitin from the blood stream of mice. Furthermore, the particles were demonstrated to be nontoxic to cultured cells (fibrosarcoma cells) over a concentration range of 3 – 3000 µg/ml. This is a very promising result for future *in vivo* measurements, but the fluorescent technique is costly and not label-free.

In this article, we will focus on detection by means of differential heat-transfer resistance. For the Heat-transfer Method (HTM) only two thermocouples, a proportional-integral-derivative (PID) controller and an adjustable heat source are required, ensuring a straightforward sensor platform and low-cost detection. This approach has been recently applied for the screening of single nucleotide polymorphisms in DNA fragments [25], which makes it a valuable tool in mutation analysis. To our knowledge, HTM has not been employed yet for small-molecule detection with MIP receptors. There are some examples of thermometric MIP sensors in literature, but they are based on the reaction heat developed upon binding and not on the heat transfer properties of the MIP-layer [26, 27, 28]. As a proof-of-principle experiment, we studied the detection of L-nicotine (Figure 1) with the HTM concept.

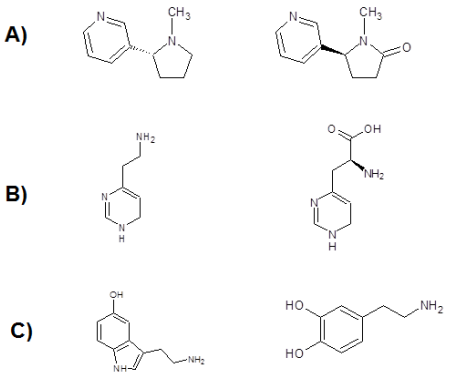

Figure 1: Chemical structures of A) L-nicotine and its metabolite cotinine B) histamine and its precursor histidine C) serotonin and its competitor dopamine.

L-nicotine is the major addictive substance in tobacco [29]. Consumption of tobacco has proven to result in a higher risk for the development of cancer [30, 31] and disorders *e.g.* pulmonary disease [32] and atherosclerosis [33]. Thoelen *et al.* [34] integrated MIP particles for L-nicotine into an impedimetric sensor setup and measured a series of concentrations in phosphate buffered saline (PBS) solutions. This MIP, based on the monomer methacrylic acid (MAA), will be used for further measurements described within this article.

The detection of histamine and serotonin in biological fluids has been reported previously with MIP receptors in combination with impedimetric read-out [20, 21]. With some slight modifications to the setup (Figure 2), we can simultaneously measure the impedance signals and heat-transfer resistance for direct validation of the results. First, proof-of-principle measurements are conducted with L-nicotine in PBS. Subsequently, similar experiments are performed with histamine and serotonin to show the principle for a variety of targets. For the applicability of the sensor platform in biological samples, spiked L-nicotine samples in saliva were studied and a dose-response curve was constructed. In summary, we will demonstrate the fast and low-cost detection of small molecules in buffer solutions with MIP receptors in combination with HTM. Since this method has the possibility of extending to biological samples, it offers a huge potential for analytical research.

2.3 Experimental

2.3.1Materials

Ethylene glycol dimethacrylate (EGDM), methacrylic acid (MAA), acrylic acid (AA), acrylamide (AM) and dimethylsulfoxide (DMSO) were obtained from Acros (Geel, Belgium). Prior to polymerization, the stabilizers in EGDM, MAA and AA were removed by filtration over alumina. The initiator azobisisobutyronitrile (AIBN) was purchased from Fluka (Buchs, Switzerland). As templates, L-nicotine, histamine and serotonin (Figure 1 A, B and C) were used. L-nicotine was obtained from Acros, while serotonin and histamine were purchased from Alfa Aesar (Karlsruhe Germany). All solvents were of analytical grade and used without further purification.

2.3.2 MIP synthesis

The MIP L-for nicotine was synthesized as follows: First, a mixture of 12.5 mmol MAA, 72 mmol EGDM and 0.61 mmol AIBN was dissolved in 7 ml hexane together with 6.41 mmol of the template molecule L-nicotine. The solution was degassed with N_2 and polymerized in a thermostatic water bath at 60 °C for 72 h. After polymerization, the polymer was ground and the L-nicotine was removed by Soxhlet extraction with methanol (48 h), a mixture of acetic acid/acetonitrile (1/1) (48 h) and again methanol (12 h). A non-imprinted polymer (NIP) was synthesized according to the same procedure, but without the presence of the target molecule. The synthesis procedure for the MIPs for serotonin and histamine are described in detail in ref [20] and [10].

2.3.3 Electrode preparation for the thermal resistance and impedance measurements

For the heat-transfer resistance and impedance measurements, 1 x 1 cm^2 aluminum substrates were spincoated with conductive OC_1C_{10}-PolyPhenyleneVinylene (PPV). This PPV derivative, serving as an adhesive layer, was synthesized via the sulfinyl precursor route [35]. Subsequently, MIP –and NIP particles were applied to the surface with a polydimethylsiloxane (PDMS) stamp. By heating above the glass transition temperature of 120 °C, the powder is allowed to sink partially into the adhesive layer. After cooling, the surface is rinsed with isopropanol to remove excessive powder and ensure that the particles are strongly fixated into the layer [34]. To demonstrate an equal load of the MIP –and NIP electrode, the sensor surface was studied with an Axiovert 40 inverted optical microscope (Carl Zeiss). With optical microscopy in combination with image processing (software by Image J of National Institute of Health, Bethesda, USA), the MIP (25 ± 2 %) and NIP (24 ± 3 %) were found to have nearly identical particle loadings which is necessary to perform differential measurements.

2.3.4 Design of sensor-setup

The general concept for the measuring setup is shown in Figure 2.

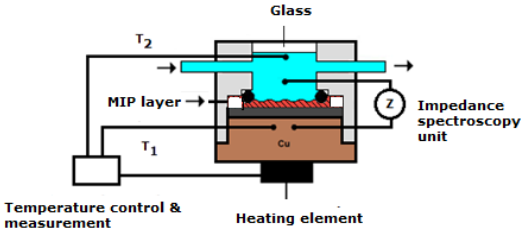

Figure 2: Schematic illustration of the general concept of the measuring set-up. The temperature of the copper block, T_1, is strictly controlled at 37.00 ± 0.02 °C. The heat flows from the copper block through the MIP-layer to the liquid, where T_2 is measured. Simultaneously with the temperature, the impedance is monitored.

The aluminum substrates, functionalized with MIP and NIP particles, were horizontally mounted into a Perspex flowcell with an internal volume of 110 µl. Silver paste ensured good thermal contact between the copper and the substrate. Two miniature thermocouples (type K, diameter 500 µm, TC Direct, the Netherlands) monitored the temperature of the copper backside contact (T_1) and the temperature of the fluid (T_2) 1.7 mm above the chip surface. The temperature T_1 was strictly controlled at 37.00 ± 0.02°C with a home-made PID controller (parameters: P = 10, I = 5, D = 0.1). Hereby, the temperature inside the human body is mimicked. For the generated heat flow, a power resistor (22 Ω, MPH20, Farnell, Belgium) was used which was mechanically attached to the copper block with heat-conductive paste. Simultaneously with the temperature, the impedance response was measured in a frequency range of 100 Hz to 100 kHz with 10 frequencies per decade and a scanning speed of 5.7 s per sweep. The amplitude of the AC voltage was fixed to 10 mV under open circuit conditions. All measurements were performed under static conditions [25].

2.3.5 Sample preparation in phosphate buffered saline (PBS) solutions for L-nicotine, histamine and serotonin

For a proof-of-principle experiment, the detection of L-nicotine was performed in PBS buffer (pH = 7.4). PBS buffer was used to simulate the ionic strength of biological samples. The L-nicotine concentrations were varied from 100 nM to 1.0 mM to ensure a wide concentration regime is analyzed. To test the selectivity, the same concentrations were prepared with cotinine in PBS. This procedure was repeated for histamine and serotonin. In the case of histamine, histidine served as an analogue while for serotonin its competitor dopamine was selected.

2.3.6 Sample preparation of spiked saliva samples

As a next step, saliva samples were analyzed. To collect the saliva, a non-smoker test person deposited saliva in a sterilized Falcon tube. The saliva was centrifuged immediately for 10 min with a speed of 10,000 rpm and the supernatant subsequently filtered with a 1 µm syringe filter. The obtained saliva samples were split into several aliquots. One aliquot was kept unaltered, thereby serving as a control fluid. The other aliquots were spiked with L-nicotine concentrations of 0.25, 0.5, 1.0, 2.5 and 10.0 mM.

2.4 Results and discussion

2.4.1 Proof-of-principle: L-nicotine measurements in buffer

The MIP –and NIP functionalized aluminum chips were mounted into the flow-cell, which was subsequently filled with PBS of pH 7.4. The flow-cell was placed in an environment with a stable ambient temperature of 19 ± 0.02 °C. The temperature of the copper, T_1, was strictly controlled at 37 ± 0.02 °C by the PID controller. When T_2 reached a stable level, increasing concentrations of L-nicotine in PBS (0.05 – 10 µM) were added. Between each addition, the sensor was left to stabilize for at least 15 min. The time-dependence of T_2 for a measurement with the MIP functionalized electrode is shown in Figure 3.

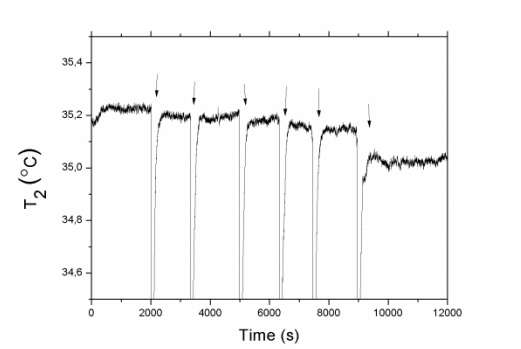

Figure 3: The temperature of the fluid (T_2) in time when the MIP is exposed to increasing concentrations of L-nicotine (0.05 -10.0 µM in PBS buffer, pH 7.4). The additions are indicated by arrows.

In PBS, T_2 stabilizes at 35.2 ± 0.02 °C. After adding increasing concentrations of L-nicotine, a drop in the temperature T_2 is observed. However, to analyze the layer properties before and after binding of the target exactly, we should not only study the effect on temperature T_1 and T_2 but also the power (P). Therefore, we propose to investigate the thermal resistance (R_{th}), as was done previously for the detection of point mutations in DNA [25]. This is defined as follows:

Equation 1 $R_{th} = \frac{T_1 - T_2}{P}$:

In this formula, ΔT corresponds to the temperature difference (T_1 - T_2) and P is the required heating power of the adjustable heat source in order to keep T_1 constant. With these parameters, the time dependent R_{th} data can be calculated. These results are shown for the MIP functionalized electrode (Figure 4A) and the electrode with only the adhesive MDMO-PPV (Figure 4B). The NIP electrode was also measured, but not included in Figure 4 since the results were very similar to the electrode with only the adhesive polymer.

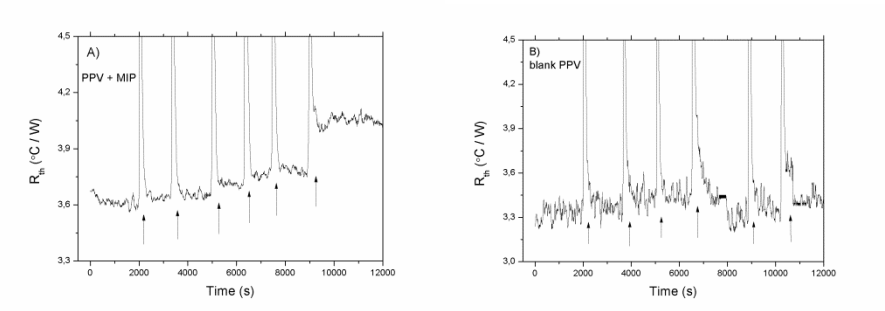

Figure 4: Time-dependence of the heat-transfer resistance R_{th} upon exposure to increasing L-nicotine in PBS (0.05, 0.1, 0.2, 0.5, 1.0 and 10.0 µM) for **A)** the MDMO- PPV-spincoated aluminum electrode functionalized with MIP particles by thermal treatment **B)** the aluminum electrode spincoated with MDMO-PPV and subsequently heated above its glass transition temperature. To all the data, a percentile filter (50% of 50 points) was applied.

Upon introducing a concentration of 10µM L-nicotine in PBS (pH 7.4), no response in R_{th} is observed for the reference system. Surprisingly, the electrode functionalized with MIP particles showed a significant increase of ~0.4 °C/W.

This can be explained qualitatively by the "pore-blocking model". MIPs contain nanopores which can specifically rebind their target based on its size and functionality. Upon rebinding, the heat flux through one cavity is strongly reduced due to the presence of the template. As a result, the total heat-transfer will be increased. The more L-nicotine will be bound, the more cavities will exhibit this behavior leading to an ultimately higher effect size. This "pore-blocking model" is schematically shown in Figure 5.

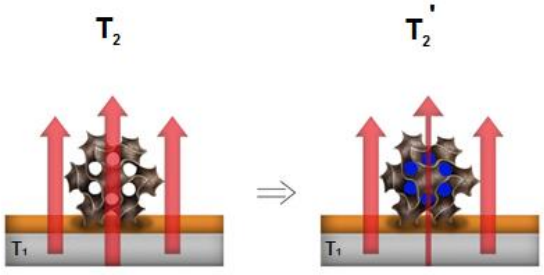

Figure 5: Artist's impression of the "pore-blocking model". The MIP particle, embedded in the surface, contains various pores where binding sites are present for its template. When these channels are filled by target molecules (indicated by blue dots), heat flux through the MIP layer is strongly reduced.

In PBS, the R_{th} stabilizes at 3.6 ± 0.1 °C/W and increases to 4.0 ± 0.1 °C/W upon addition of 10 µM of L-nicotine (Figure 4B). The effect size of ~11.0% is significantly higher than the noise on the signal (3%), thereby directly proving the binding of the target to the nanocavities of the MIP. These experiments were now performed with freshly prepared electrodes in the concentration regime 0 – 100 µM L-nicotine in PBS. In order to demonstrate specificity of the sensor platform, the same measurements were also conducted with the NIP-functionalized electrode. Additionally, the effect of cotinine (Figure 1A) additions on the MIP was analyzed. This was done in order to address the selectivity, as cotinine is similar in chemical structure and L-nicotine's

natural metabolite. The R_{th} data can be represented as a dose-response curve, where the difference in R_{th} versus the concentration of the target is plotted. These results are summarized in Figure 6.

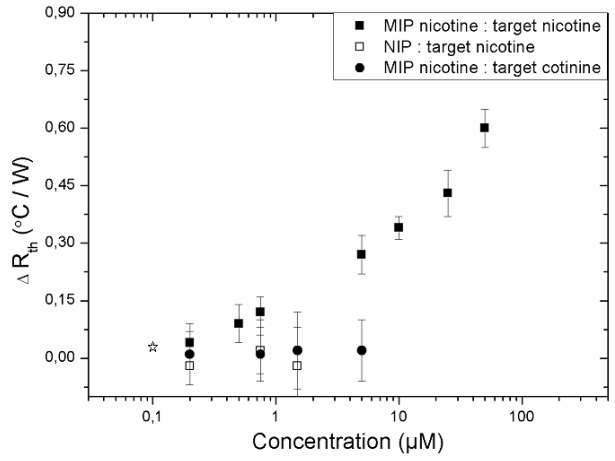

Figure 6: Dose-response curve for the MIP (solid squares), NIP (open squares) and MIP with cotinine (solid circles), where ΔR_{th} is plotted versus the logarithm of the target concentration. The target concentration of L-nicotine and cotinine varies from 0 – 100 µM in PBS (pH 7.4). The asterisk corresponds to the limit of detection, below this concentration there is no significant response of the MIP to L-nicotine.

The measurements were performed in threefold; each measurement was conducted with a freshly functionalized electrode. The error bars given in Figure 6 correspond to the standard deviation on the three separate experiments, showing excellent inter reproducibility of the samples. We could measure in a wide concentration regime, from 0.2 µM (ΔR_{th} = 0.07 ± 0. 01 °C/W) to 50 µM (ΔR_{th} = 0.60 ± 0. 03 °C/ W). The standard deviation at baseline-level, when no L-nicotine is present (0.01 °C/W) is used to estimate the detection limit, which is commonly defined as the concentration where the signal amplitude is three times the standard deviation. In the low concentration regime, 0.2 – 0.75 µM, the dose-response results can be represented well with a linear fit (R^2 = 0.97). With this fit, the limit of detection was calculated to be approximately 125 nM. This is within the physiologically relevant range, the L-nicotine saliva concentration can vary from 0 – 500 µM [36]. The sensing platform was also determined to be specific, since the NIP with L-nicotine and the MIP with cotinine did not show a significant response in R_{th}.

2.4.2 L-nicotine in buffer : validation by impedance spectroscopy

After stabilizing in PBS, increasing concentrations of L-nicotine and cotinine were added (0 – 1000 µM). Between the addition steps the sensor was left to stabilize for 10 min. Subsequently, the response value was obtained by averaging five impedance data points with an interval of one minute. All the obtained impedance data were normalized with respect to a starting value of 100 % pure PBS. The corresponding dose-response curves at a frequency 316 Hz are shown in Figure 7. This frequency was selected because it is low enough to probe capacitive effects and ensures a high signal to noise ratio [33]. The impedance was measured simultaneously with the heat-transfer resistance, meaning Figure 6 and Figure 7 show the results of the same experiments but obtained with a different read-out technique.

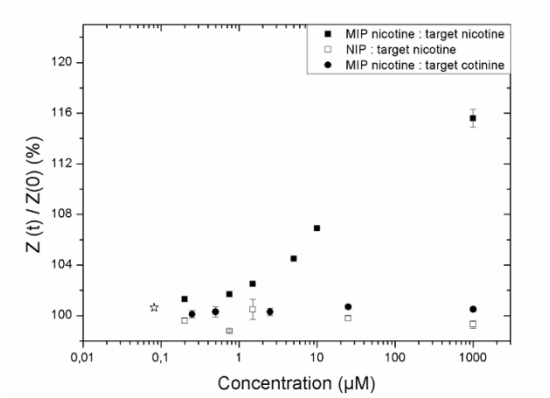

Figure 7: Dose-response curve at 316 Hz for the MIP (solid squares), NIP (open squares) and MIP with cotinine (solid circles), where the normalized impedance is plotted versus the logarithm of the target concentration. These experiments were performed simultaneously with the heat-transfer measurements, which results are shown in Figure 6. The concentration varies from 0 – 1000 µM of L-nicotine or cotinine in PBS (pH 7.4). The error bars are indicated, but might be smaller than symbol size.

Without the presence of L-nicotine, the standard deviation on the signal was 0.2%. This would correspond to a detection limit of approximately 100 nM, which is comparable to what was achieved with HTM. For the MIP, a linear response in R_{th} is observed from 0.1 – 2.5 µM L-nicotine. At higher concentrations saturation is gradually occurring, the maximum response of 115.6 ± 0.7 % is obtained at 1000 µM. For comparison, the NIP signal did not significantly change upon exposure to concentrations of L-nicotine while the increase of the MIP to 25 µM cotinine was only 100.7 ± 0.2%. This corroborates the heat-transfer results, validating that the sensor platform can be applied for the specific detection of L-nicotine in buffer solutions.

2.4.3 Histamine and serotonin measurements in buffer

To demonstrate the applicability of the sensor platform for a variety of target molecules, additional histamine and serotonin measurements (0 – 1000 µM in PBS of pH 7.4) were performed with MIP materials presented in previous work [10, 20]. As analogues, we selected for histamine its precursor histidine (Figure 1B) and for serotonin its natural competitor dopamine (Figure 1C). The dose-response curves are shown in Figure 8.

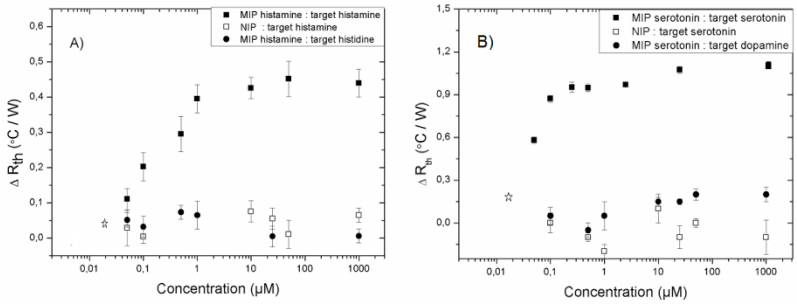

Figure 8: A) Dose-response curve for the MIP of histamine (solid squares), NIP (open squares) and MIP with histidine (solid circles), where ΔR_{th} is plotted versus the logarithmic target concentration. The target concentration varies from 0.2 –1000 µM in PBS (pH 7.4). **B)** Dose-response curve for the MIP of serotonin (solid squares), NIP (open squares) and MIP with dopamine (solid circles), where ΔR_{th} is plotted versus the logarithmic target concentration. The concentrations in PBS vary from 0.2 – 1000 µM.

Figure 8A shows the dose-response curve for histamine. At a maximum concentration of 1000 µM histamine, the ΔR_{th} of the MIP increased with 0.4 ± 0.04 °C/W. Its references, the NIP with histamine and the histamine MIP with histidine as target, showed no significant response at this concentration range. Thereby, it is proven that the sensing platform can detect histamine in a specific manner. Furthermore, we estimated the detection limit to be approximately 30 nM, which is within the range as was obtained previously with impedance spectroscopy [21].

From Figure 8B can be determined that upon addition of 50 µM serotonin, the R_{th} of the MIP goes up by 1.07 ± 0.03 °C/W. There was no effect on the NIP, some minor increases occurred for the serotonin MIP in combination with the competitor dopamine (0.2 ± 0.05 °C/W). However, the signal ratio between target versus competitor is approximately 5, which ensures selective detection of serotonin with the sensor platform. The estimated limit of detection is 20 nM, low enough to measure in the physiologically relevant concentration range [20].

The detection limits of the HTM and impedimetric read-out for various target are summarized in Table 1. Furthermore, the biologically relevant concentration range is given.

Table 1: LOD in 1x PBS with HTM and impedimetric read-out compared to the biologically relevant concentration

	1 x PBS		**Biological samples**		
Target	**LOD HTM**	**LOD Impedance**	**Saliva**	**Urine**	**Blood**
L-nicotine	100° nM	100	0.2 – 1000 µM [36]	0.3 – 10 µM [34]	-
serotonin	20 nM	5 nM [20]	-	-	10 – 1500 nM [20]
histamine	30 nM	15 nM [21]	-	200 -750 nM [10]	10 – 1000 nM [10]

2.4.4 Proof of application: detection of L-nicotine in spiked saliva samples

In order to assess the applicability of the sensor platform in biological media, saliva samples spiked with L-nicotine (0.25, 0.5, 1.0, 2.5 and 10.0 mM) were evaluated. For these measurements there was no need for dilution, thereby further simplifying the sample preparation. The absolute R_{th} values for the MIP and NIP after exposure to increasing spiked concentrations of L-nicotine are shown in Figure 9.

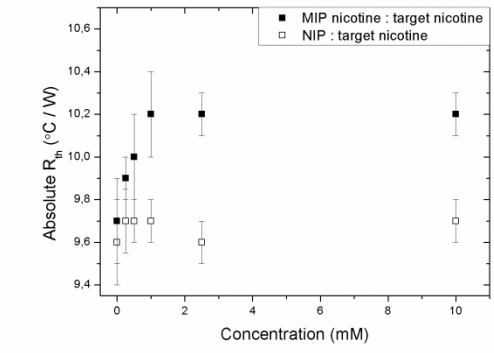

Figure 9: The dose-response curve for the concentration of L-nicotine in spiked saliva (0, 0.25, 0.5, 1, 2,5, 10 mM) versus the differential heat-transfer resistance (ΔR_{th}). This curve represents the absolute values of the R_{th} of MIP and NIP.

The absolute R_{th} values in saliva are higher than for the L-nicotine MIP in PBS. This can be due to two reasons; first, the absorbed proteins act as an additional insulating layer, increasing the total thermal resistance and, second, the viscosity of the saliva is much higher which limits the heat-transport and prolongs measurement time.

Figure 9 shows that there was no significant response of the NIP to increasing concentrations of spiked L-nicotine. For the MIP, in the regime from 0.25 to 1.0 mM the increase in ΔR_{th} is linear (R^2 = 0.97) with a maximum of 0.5 ± 0.01 °C/W. For concentrations higher than 1.0 mM, saturation is occurring due to increasing occupation of the binding sites. The sensitive regime of the sensor is between 0.25 to 1.0 mM and these concentrations are within the relevant range of biological samples [36]. Therefore, the applicability of the sensor platform for measurements in biological samples is demonstrated.

In the case of saliva, no reference impedance tests could be conducted. This is due to the absorption of proteins, resulting in an extremely high electrical resistance beyond the measuring limit. While we could not directly validate the results, this might be an additional benefit for the R_{th} based sensor platform as we can also measure in complicated viscous solutions.

2.5 Conclusions

In this article, we presented the heat-transfer method (HTM) for the specific detection of L-nicotine. This is the first time detection of small molecules based on MIP-type receptors in combination with the HTM concept has been reported. The principle of the technique can be explained by the "pore-blocking model" ; upon binding of the target to the nanocavities present in the MIP, heat transport in that direction is strongly reduced resulting in a total increase of the heat-transfer resistance. For proof-of-principle measurements, L-nicotine concentrations in PBS solutions were analyzed. The detection could be performed in a specific manner, which was validated by reference tests with impedimetric read-out. In addition, a similar detection limit was achieved compared to the impedance spectroscopy tests. This detection limit is surprising low, it is in the nanomolar range which is well within the physiologically relevant regime. Furthermore, it was possible to extend this method to other small molecules, which was proven for histamine and serotonin samples in buffer solutions. As a first proof-of-application experiment, saliva samples spiked with L-nicotine were evaluated. The constructed dose-response curve showed sensitivity in the physiologically relevant regime, demonstrating the applicability of the sensor platform in biological media. Summarizing, the novel approach HTM enables the fast, straightforward, and low-cost detection of small molecules with MIP-receptors which makes it of great interest for biosensing and analytical applications.

2.6 Acknowledgements

This work is supported by the Life-Science Initiative of the Province of Limburg (M. Peeters) and by the Internationalization Program of Universidade de São Paulo, Brazil (P. Csipai). The authors also would like to thank A. Gaulke and P. Losada-Pérez for stimulating scientific discussions and H. Penxten, J. Soogen, C. Willems, and J. Baccus for technical assistance.

2.7 References

[1] Mosbach K, *Trends Biochem Sci*, 1994, **19,** 9-14.

[2] Arshady R, Mosbach K, *Chem Phys*, 1981, **182,** 687-692.

[3] Shi H, et al., *Nature*, 1999, **398**, 593-597.

[4] Hayden O, Lieberzeit PA, Blaas D, Dickert FL, *Adv Funct Mater*, 2006, **16**, 1269-1278.

[5] Hayden O, Mann KJ, Krassnig S, Dickert FL, *Angew Chem Int Ed*, 2006, **45**, 2626-2629.

[6] Jenik M, Seifner A, Lieberzeit PA, Dickert FL, *Anal Bioanal Chem*, 2009, **394**, 523-528.

[7] Wulff G, *Trends Biotechnol*, 1993, **11**, 85-87.

[8] Vlatakis G, Andersson LI, Müller R, Mosbach K, *Nature*, 1993, **361**, 645-647.

[9] Owens K, Karlsson L, Lutz ESM, Andersson LI, *Trends Anal Chem*, 1999, **18**, 146-154.

[10] Horemans F, et al., *Sens Actuators B*, 2010, **148**, 392-398.

[11] Vaihinger D, et al., *Macromol Chem Phys*, 2002, **203**, 1965-1973.

[12] Stobiecka M, Deeb J, Hepel M, *ECS Trans*, 2009, **19**, 15-32.

[13] Haupt K, Mosbach K, *Chem Rev*, 2000, **100**, 2495-2504.

[14] Benito-Pena E, et al., *J Chromatogr A*, 2008, **1208**, 62–70.

[15] Andersson LI, et al., *J Chromatogr*, 1990, **516**, 323–331.

[16] Vidyasankar S, Ru M, Arnold FH, *J Chromatogr A*, 1997, **775**, 51-63.

[17] Avila M, Zougagh M, Escarpa A, Rios A, *Trends Anal Chem*, 2008, **27**, 54–65.

[18] Piletsky SA, Turner, APF, *Electroanalysis*, 2002, **13**, 317-323.

[19] Mao Y, et al., *Bios. Bioelectron*, 2011, **28**, 291-297.

[20] Peeters M, et al., *Sens Actuators, B*, 2012, **171-172**, 602-610.

[21] Peeters M, et al., *Anal. Chem*, 2013, **85**, 1475-1483.

[22] Patel AK, Sharma PS, Prasad BB, *Thin Solid Films*, 2010, **10**, 2847–53.

[23] Prasad BB, Srivastava S, Tiwari K, Sharma PS, *Biochem Eng J*, 2009, **44**, 232–9.

[24] Hoshino Y, et al., *J Am Chem Soc*, 2010, **132**, 6644-6645.

[25] Van Grinsven B, et al., *ACS Nano*, 2012, **6**, 2712-2721.

[26] Athikomrattanakul U, et al., *Anal Chem*, 2011, **83**, 7704-7711.

[27] Lettau K, et al., *Angew Chem Int Edit*, 2006, **45**, 6986-6990.

[28] Rajkumar R, et al., *Biosens Bioelectron*, 2008, **23**, 1195-1199.

[29] Neal LB, *Prev Med*, 1997, **26**, 412–417.

[30] Schrek R, Baker LA, Ballard GP, Dolgoff S, *I. Cancer. Cancer Res*, 1950, **10**, 49–58.

[31] Doll R, Peto R, *JNCI*, 1981, **66**, 1191-1308.

[32] Mayer AS, Newman LS, *Respir Physiol*, 2001, **128**, 3–11.

[33] Bergström J, *Odontology*, 2008, **92**, 1–8.

[34] Thoelen R, et al., *Biosens Bioelectron*, 2008, **23**, 913-918.

[35] Louwet D, Vanderzande J, Gelan A, *Synth Met*, 1995, **69**, 509-510.

[36] Russell MA, et al., *Br Med J*, 1976, **6017**, 1043-1046.

Chapter 3

Implementing heat transfer resistivity as a key element in a nanocrystalline diamond based single nucleotide polymorphism detection array

Diamond and Related Materials, 2013, **Under Review**

K. Bers[1], B. van Grinsven[1], T. Vandenryt[1,2], M. Murib[1], W. Janssen[1,3], **B. Geerets[1]**, M. Ameloot[4], K. Haenen[1,3], L. Michiels[4], W. De Ceuninck[1,3], and P. Wagner[1,3]

1) Hasselt University, Institute for Materials Research, Wetenschapspark 1, B-3590 Diepenbeek, Belgium
2) XIOS University College, Department of Applied Engineering, Agoralaan - Building H, B-3590 Diepenbeek, Belgium
3) IMOMEC, Wetenschapspark 1, 3590 Diepenbeek, Belgium
4) Hasselt University, Biomedical Research Institute, Agoralaan, B-3590 Diepenbeek, Belgium

3.1 Abstract

In this article, we report on the label-free real-time thermal monitoring of the denaturation of specific DNA fragments and its potential to detect and quantify single nucleotide polymorphisms (SNPs). Probe DNA, consisting of a 36-mer fragment was covalently immobilized on nanocrystalline chemical vapour deposition (CVD) diamond platforms and hybridized with a 29-mer target DNA fragment (full matching and/or with a point mutation). It was observed that the change in heat transfer resistance upon denaturation is dependent on the amount of DNA hybridized to the nanocrystalline diamond (NCD) surface. Furthermore the possibility to distinguish between a full matching sequence and its singularly mutated counterpart, when bound to the same NCD surface, was investigated. NCD surfaces were selectively hybridized with both full matching and mutated DNA fragments at different ratios (3:1, 2:2 and 1:3). A clear bipartite response in heat transfer resistivity was observed upon simultaneous denaturation of these DNA fragments. Denaturation temperature could be used to identify the DNA fragment to which each partial response could be attributed. Moreover, the partial increases in heat transfer resistivity related to the hybridized amount of non-mutated or mutated DNA, respectively. These results imply that heat transfer resistivity is a technique which can be used to (i) quantify DNA fragments of interest, (ii) detect and (iii) quantify SNPs in a mixture of mutated and non-mutated DNA fragments. Moreover, it illustrates the potential of this technique to detect SNPs without the necessity to design complex microarrays.

3.2 Introduction

Diamond has proven to be an excellent platform for biomedical research due to its outstanding material properties such as chemical inertness, thermal conductivity, and electronic properties [1]. In addition, intrinsic diamond displays a high chemical and electrochemical stability and has a wide band gap (5.5 eV) [2-4]. In recent years there has been a major development of DNA electrochemical biosensors such as field-effect sensors [5-7] and sensors monitoring electrical surface properties such as conductance, resistance [8] and capacitance [9]. In addition, diamond proved to be a good transducer for protein sensing as well [10-12]. In previous work it was established that the monitoring of changes in heat transfer resistance of double stranded DNA (dsDNA), which was single stranded covalently bound to a nanocrystalline diamond (NCD) surface, upon denaturation is an interesting approach to measure duplex stability and as such discriminate between different DNA sequence fragments [13]. The change in heat transfer resistance upon denaturation of the dsDNA to ssDNA was hypothesized to be due to the difference in geometrical configuration between dsDNA and ssDNA, which is, respectively, collapsed or erected on the surface. Elaborating on these results this study focuses on the effect size of heat transfer resistance changes as a function of the attached amount of target DNA. For this purpose, hybridization was restricted to a range of specific areas of the NCD surface. To do so, a PDMS flow cell was designed to divide the NCD surface in four identical and fully isolated areas, in which hybridization could take place. The change in heat transfer resistance in response to denaturation was analysed in function of hybridization surface coverage (25, 50, 75 or 100 %). Secondly, it is investigated if one can distinguish between a full matching sequence and a point mutated sequence when bound to the same NCD surface. The same PDMS flow cell was used to selectively hybridize NCD surfaces with full matching DNA fragments and singularly mutated sequences at different ratios (3:1, 2:2 and 1:3). It was investigated whether the theoretical difference in stability between the two types of DNA fragments would also translate into a two-step response in heat transfer resistance upon denaturation. The aim of this article is to gain insight in the surface coverage to effect size ratio as an analogue to a dose response curve and to show an early stage DNA micro-array where one can identify two different sequences with different melting temperatures by means of only two thermocouples and an adjustable heat source.

3.3 Experimental

3.3.1 Synthesis of nanocrystalline diamond

10 × 10 mm^2 doped (10–20 kΩcm) p-type crystalline silicon wafers (100) were seeded with a water-based colloid of ultra-dispersed detonation (nano)diamond. NCD films with thicknesses of ~ 300 nm and grain sizes of 100 nm were grown on this silicon substrate, using microwave plasma-enhanced chemical vapour deposition (MPECVD) in ASTEX reactor equipped with a 2.45 GHz microwave generator. This is achieved by using a standard mixture of 15 sccm methane gas (CH_4) and 485 sccm hydrogen gas (H_2) to deposit the NCD thin films on the silicon wafer. The growth was performed under a pressure of 45 Torr, and temperature of 750 °C, the microwave power was set to 4000 W. The growth rate was ~ 390 nm/h.

3.3.2 Sample preparation

Probe DNA, consisting of a 36-mer single stranded DNA (ssDNA) fragment (3'-CCA AGC CCC CAT ATG TAC CCG ACG TCC CC - A AAA AAA C_6H_{12}-NH_2-5') was covalently immobilized on NCD electrodes. First, the diamond surface is hydrogenated. The hydrogenation is done at 700 °C during 30 s at 3500 W, 12 kPa and 1000 sccm hydrogen gas (H_2) [14]. After hydrogenation the samples are placed inside a glovebox under nitrogen atmosphere. The hydrogenated NCD is then covered with a thin film of unsaturated fatty acid (10-undecenoic acid) and exposed to UV radiation (254 nm, 265 mW/cm^2) for 20 hours under nitrogen atmosphere. The double bonds of the unsaturated fatty acid chains will break and a covalent bond with the hydrogen-terminated diamond is established. This process is mediated by photoemission from the surface as proposed for the photochemical grafting of alkenes to silicon surfaces [3,4]. The fatty acid layer is about 2 nm thick [15]. The unbound fatty acid chains are washed off using acetic acid and milliQ water at 120 °C. In this way a carboxyl (COOH) terminated NCD surface is obtained. Zero-length 1-ethyl-3-[3-dimethylaminopropyl]-carbodiimide (EDC) is used for the covalent coupling of the 5' side of an amino-modified 36-mer ssDNA fragment to the carboxyl-terminated surface in 2-[N-morpholino]-ethannesulphonic acid (MES) buffer at 4 °C.

3.3.3 PDMS flow cell

A mold is fabricated in Teflon (PTFE) to serve as the master template, through numerical control milling. Four identical triangles, which occupy an area of 10 mm^2 each, with a height of 1 mm are cut from a PTFE block, as can be seen in **Figure 1**. The master mold is then encapsulated in uncured polydimethylsiloxane (PDMS) polymer (Sylgard 184, Dow Corning), which is mixed in a 10:1 ratio with the curing agent. The mixture is degassed for 30 minutes at an absolute pressure of 50 kPa, to remove trapped gas bubbles. Curing of the PDMS in an oven at 120 °C takes approximately 20 minutes. The cured daughter-mold can be gently peeled from the master template and cut to the required dimensions with a lancet. A biopsy punch (Miltex) with a 1 mm inner diameter is used to core both an inlet and outlet as connection ports for each triangular cavity. PTFE tubing (1.2 mm outer diameter) is press-fitted in the connection ports [16], to form a reliable connection without additional bonding or molding. Finally, the PDMS mold is pressed onto the diamond covered silicon substrate. As such it provides four completely separated identical areas for hybridization on the NCD sample.

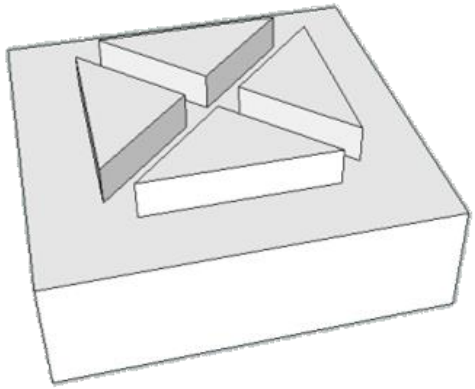

Figure 1: CAD drawing of the flow cell master mold.

3.3.4 Selective hybridization

In a following step, 6 µl FAM-488-modified ssDNA is mixed with 14 µl 1× PCR buffer and selectively added to specific areas of the ssDNA-modified NCD sample by means of the PDMS flow cell. The sample is then incubated at 35 °C for 2 hours for hybridization to take place. Non-specifically bound DNA is removed using a double washing step. In a first step, the sample is washed with 2× saline sodium citrate (SSC) + 0.5 % sodium dodecyl sulphate (SDS) for 30 minutes. Secondly, the sample is washed twice with 0.2× SSC at 30 °C for 5 minutes. Finally, the sample is rinsed with phosphate buffered saline (PBS) of pH 7.2 and stored in PBS at 4 °C [2]. The use of low salt concentrations in comparison to the hybridization buffer and by washing at temperatures lower than hybridization temperature, premature denaturation is avoided. Both full match ssDNA fragments (5'-GGT TCG GGG GTA TAC ATG GGC TGC AGG GG-3') and ssDNA fragments with a point mutation at position 20 (5'-GGT TCG GGG **C**TA TAC ATG GGC TGC AGG GG-3') were used for hybridization.

3.3.5 Fluorescence imaging

Fluorescence images were taken on a Zeiss LSM 510 META Axiovert 200 M laser scanning confocal fluorescence microscope. To excite the FAM-488 fluorescence dye, a 488 nm argon-ion laser was used with a maximum intensity at the sample surface of 30 µW to avoid bleaching during the image acquisition. The peak emission has a longer wavelength of 518 nm due to vibrational relaxation of the FAM molecule after photon absorption. All images were collected with a 10 × 0.3 Plan Neofluar air objective with a working distance of 5.6 mm. The pinhole size was 150 µm and the laser intensity was set at 10 %. The detector gain, being a measure for the photomultiplier voltage in arbitrary units, was set to 950. The fluorescent intensity was analysed using ImageJ software.

3.3.6 Experimental setup

The general principle of the heat-transfer method is shown in **Figure 2.** The central element of the platform consists of an adjustable heat source attached to a copper block that transfers a thermal current trough the NCD chip (1 by1 cm^2), selectively hybridized with DNA. During measurements, the temperature above the NCD chip, T_1, is stringently stabilized with a PID controller and the temperature T_2, in the liquid compartment underneath the NCD, is monitored. From the temperature difference $T_1 - T_2$ and the required heating power P to keep the copper block at the selected temperature, one can derive the heat transfer resistance from $R_{th} = (T_1 - T_2) / P$ [17, 18]. The contact area between the chip and the liquid compartment was 28 mm^2.

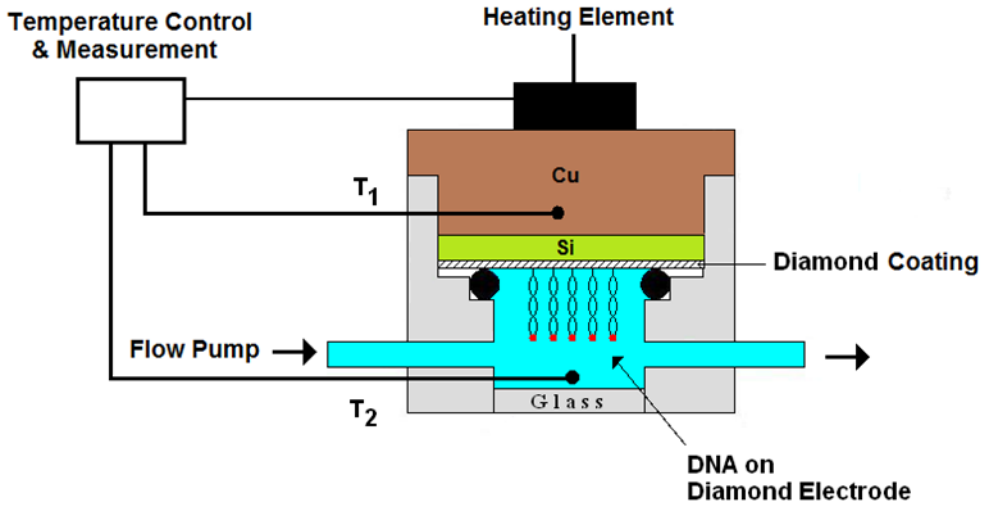

Figure 2: Schematic layout of the sensor cell, allowing for the thermal monitoring of DNA denaturation. The probe DNA is covalently immobilized on a diamond-coated silicon electrode while the cell is filled with PBS buffer. The temperature T_1 of the Cu backside contact is measured by a thermocouple and can be actively steered via a controller unit. The temperature T_2 inside the liquid is recorded by using a second thermocouple.

3.3.7 Surface coverage to effect size ratio

Diamond-coated silicon electrodes used were denoted as #D1, #D2 and #D3. In this experiment only fully complementary DNA fragments were used for hybridization. The PDMS flow cell was used to limit hybridization to distinct parts of the NCD surface by performing hybridization in one, two, three or four out of four hybridization chambers. Hybridization was performed on 25% of the occupational zone (10 mm^2) for sample #D1, 50 % (20 mm^2) for sample #D2, 75 % (30 mm^2) for sample #D3 and sample #D1 was reused to hybridize 100 % of the occupational zone (40 mm^2). During the measurement, T_1 was increased with a heating rate of 1 °C/min from 35 °C to 90 °C and cooled back to 35 °C at the same rate by reducing the heating power. This was performed for two consecutive heating/cooling runs.

3.3.8 SNP detection array

The second series of experiments refers to a combination of fully complementary duplexes and mismatched duplexes hybridized on the same NCD coated electrode. Goal of this experiment was to evaluate if discrimination between full matching DNA sequences and mutated sequences is possible based on heat transfer resistivity changes upon denaturation, when hybridized to the same sample. The PDMS flow cell provided four separated hybridization areas and as such could be used to hybridize full matching sequences (FM) on the one hand and singularly mutated sequences (1MM) on the other hand simultaneously on separated distinct parts of the NCD surface. This to provide unbiased hybridization of both types of DNA fragments. Sample #D1 was hybridized with full matching sequences and singularly mutated sequences at a FM:1MM ratio of 3:1, hybridized sample #D2 at a FM:1MM ratio of 2:2 and finally hybridized sample #D3 at a FM:1MM ratio of 1:3, in the PDMS flow cell. After the samples were mounted into the setup, T_1 was increased with a heating rate of 1 °C/min from 35 °C to 90 °C and cooled back to 35 °C at the same rate by reducing the heating power.

3.4 Experimental results

3.4.1 Surface coverage to effect size ratio

Figure 3 shows fluorescent images of samples #D1, #D2, #D3 when **(a)** 25 %, **(b)**, 50 %, **(c)** 75 % and **(d)** 100 % of the occupational zone is hybridized. After the samples were mounted into the setup, T_1 was increased with a heating rate of 1 °C/min from 35 °C to 90 °C.

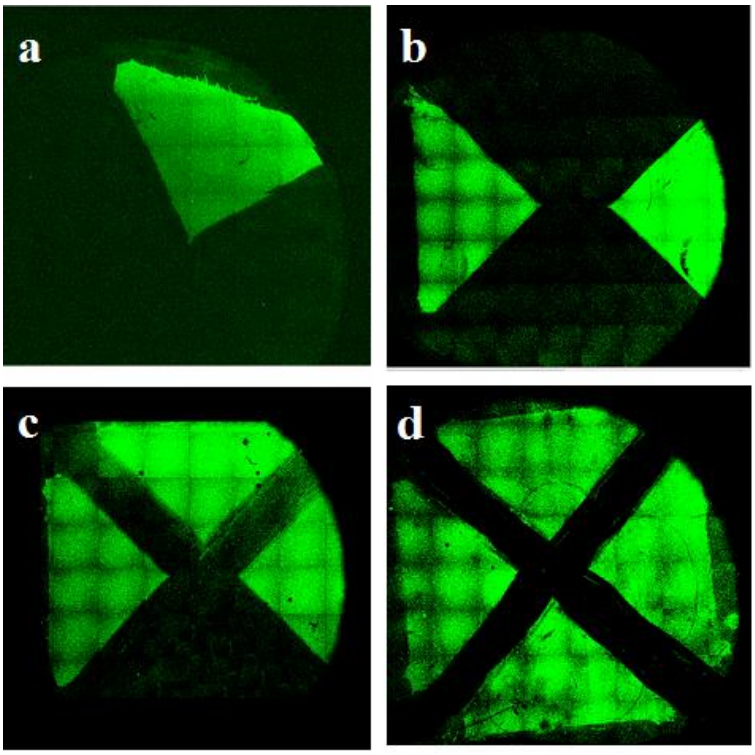

Figure 3: Fluorescent images of NCD samples #D1, #D2, #D3 when **(a)** 25 %, **(b)**, 50 %, **(c)** 75 % and **(d)** 100 % of the occupational zone is hybridized.

Figure 4 shows heat transfer resistance R_{th} as a function of temperature for electrode #D1, #D2, #D3 (data have not been filtered), when partially or fully hybridized. It can be seen that when 100 % of the occupational zone is hybridized the intial R_{th} value of double stranded DNA (black line) lies around 7 °C/W ± 0.08 °C/W and switches to 8.5 °C/W ± 0.07 °C/W upon denaturation with an inflection point in R_{th} at a temperature of 61.0 °C ± 0.1 °C. When hybridizing 75 % of the occupational zone (red line) the initial R_{th} value starts around 7.5 °C/W ± 0.11 °C/W and also switches to 8.5 °C/W ± 0.08 °C/W upon denaturation with an inflection point in R_{th} at an identical temperature of 61.0 °C ± 0.1 °C. Covering 50 % of the occupational state (blue line) leads to an initial R_{th} value of 8 °C/W ± 0.10 °C/W which increases to 8.7 °C/W ± 0.08 °C/W upon denaturation and when using only 25 % of the occupational zone (grey line) one can find an initial R_{th} value of 8.5 °C/W ± 0.07 °C/W which increases to 8.9 °C/W ± 0.08 °C/W upon denaturation.

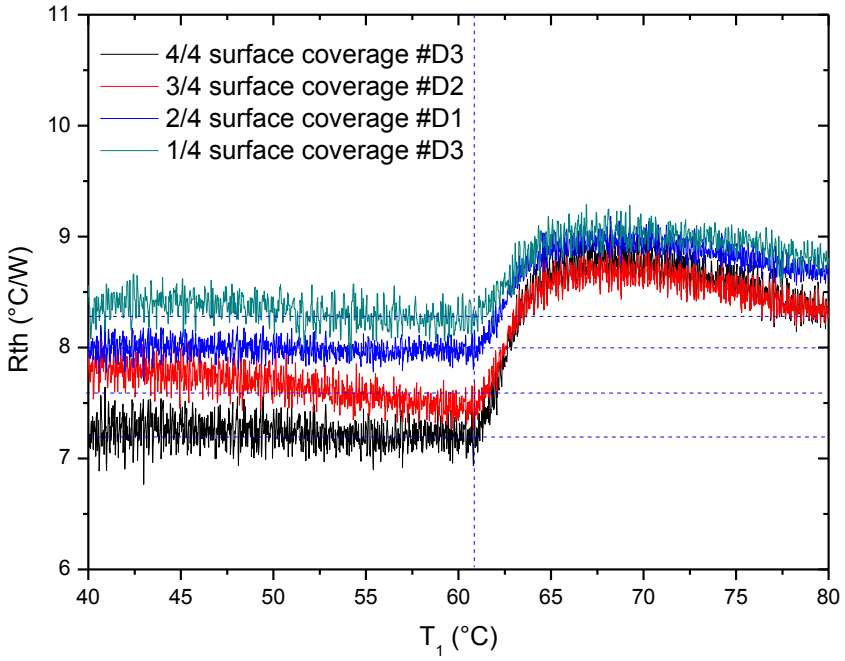

Figure 4: Heat transfer resistance R_{th} as a function of temperature when 100 %, 75 %, 50 % and 25 % of the occupational zone of a NCD sample is hybridized.

3.4.2 SNP detection array

Figure 5 shows confocal images of the second series of experiments. First we selectively hybridized sample #D1 with full matching sequences and mutated sequences at a FM:1MM ratio of 3:1 as depicted in **figure 5a**, then sample #D2 was hybridized at a FM:1MM ratio of 2:2 as shown in **figure 5b** and finally **figure 5c** shows sample #D3, hybridized at a FM:1MM ratio of 1:3. After the samples were mounted into the setup, T_1 was increased with a heating rate of 1 °C/min from 35 °C to 90 °C and cooled back to 35 °C at the same rate by reducing the heating power, this was done for two consecutive runs.

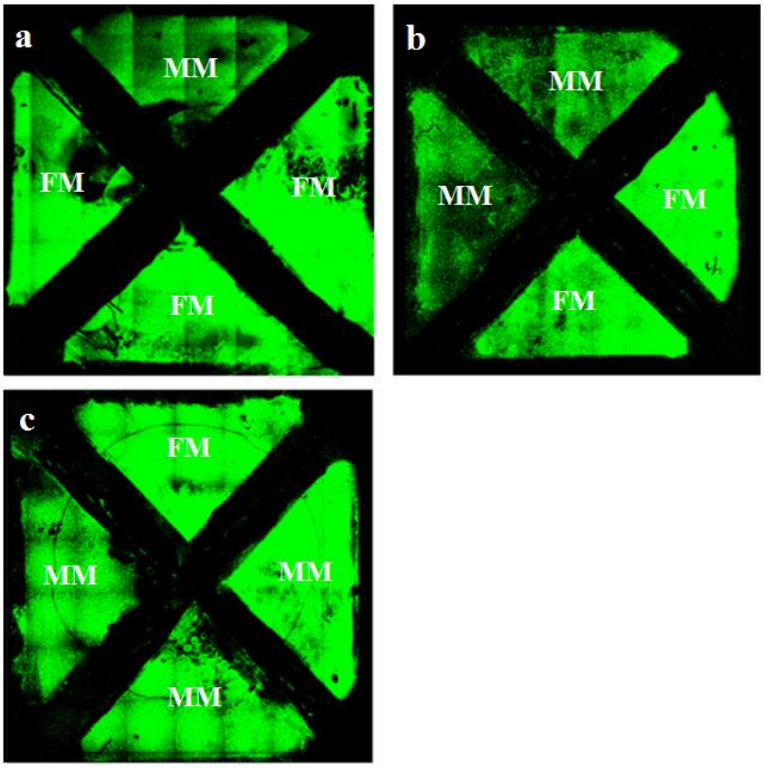

Figure 5: Fluorescent images of NCD samples #D1, #D2, #D3 when the sample is selectively hybridized with a combination of full matching sequences and mutated sequences at a ratio of (FM:1MM) (a) 3:1, (b) 2:2 and (c) 1:3.

Figure 6 shows the correlating heat transfer resistance R_{th} as a function of temperature. It can be seen that when hybridizing a NCD sample with full matching sequences and mutated sequences at a ratio of 3:1, the intial R_{th} value starts around 6.9 °C/W, then increases to 7.5 °C/W ± 0.08 °C/W with an inflection point in R_{th} at a temperature of 55.0 °C ± 0.1 °C (denaturing of the mutated sequences), stabilizes and finally shows a second increase to 8.6 °C/W ± 0.12 °C/W (denaturing of the full matching sequences) with an inflection point in R_{th} at a temperature of 61.0 °C ± 0.1 °C (**Figure 6a**). When hybridizing at a ratio of 2:2, a similar process is observed. The intial R_{th} value starts around 7.0 °C/W, but then increases to 7.8 °C/W with an inflection point in R_{th} at a temperature of 55.0 °C ± 0.1 °C, stabilizes and finally shows a second increase in to 8.6 °C/W ± 0.13 °C/W with an inflection point in R_{th} at a temperature of 61.0 °C ± 0.1 °C (**Figure 6b**). After hybridisation at a ratio of 1:3, identical R_{th} inflection point temperatures are found, but now a first increase in R_{th} is observed from 7.5 °C/W ± 0.09 °C/W to 8.5 °C/W ± 0.10 °C/W and a second increase is found from 8.5 °C/W ± 0.09 °C/W to 9.0 °C/W ± 0.11 °C/W (**Figure 6c**).

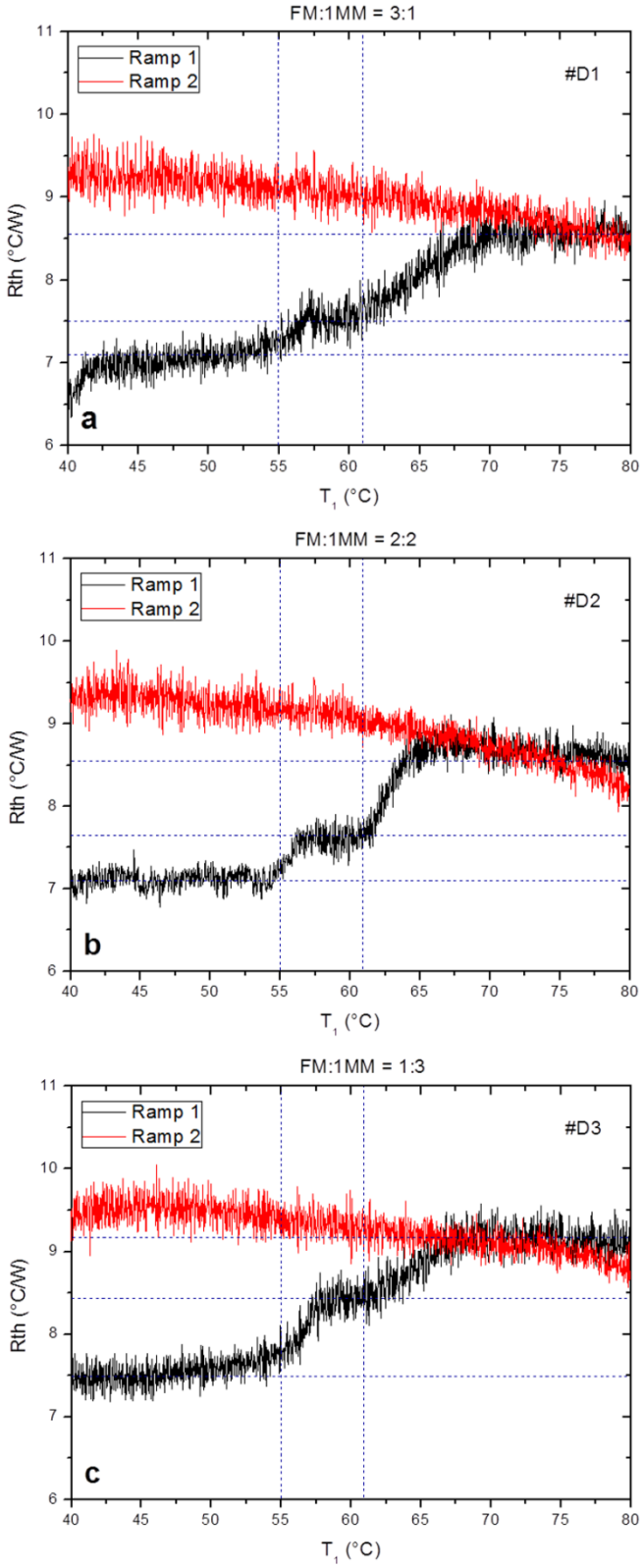

Figure 6: Heat transfer resistance R_{th} as a function of temperature, when hybridizing a NCD sample with full matching sequences (FM) and mutated sequences (1MM) at a FM:1MM ratio of 3:1 (a), 2:2 (b) and 1:3 (c). The temperature for which denaturation is initiated is marked in the graphs with a dotted line for both the mutated sequence (55 °C) and the fully matching sequence (61 °C).

3.5 Discussion

The results show that the heat transfer resistance of NCD samples increases when less DNA is hybridized to the surface. This effect can be explained by the increased proportion of non-hybridized ssDNA on the surface, which coincides with a lower hybridization surface coverage. ssDNA probes were previously reported to exhibit a higher heat transfer resistance than hybridized dsDNA fragments [13]. This difference was hypothesized to be due to the difference in geometrical configuration between the non-hybridized and hybridized DNA fragments, which are, respectively, collapsed or erected on the surface. As a consequence, since the increase in heat transfer resistance upon denaturation is due to the conversion of dsDNA to ssDNA, also a lower change in R_{th} is identified upon denaturation of samples with a low hybridization surface coverage. As is illustrated in **Figure 6**, a heat transfer resistance effect size (ΔR_{th} (%), calculated as % ΔR_{th} = ($< R_{th(70\text{-}80°C)} >$ - $< R_{th(40\text{-}60°C)} >$) / $< R_{th(40\text{-}60°C)} >$) × 100, with $< R_{th(40\ °C\text{-}60\ °C)} >$ the average heat transfer resistance before denaturation is initiated and $< R_{th(70\ °C\text{-}80\ °C)} >$ the average heat transfer resistance after denaturation has occurred), of 7.21 ± 1.45 %, 10.72 ± 0.97 %, 13.67 ± 1.84 % and 18.94 ± 1.71 % was brought about upon denaturation for 25 % (10 mm^2), 50 % (20 mm^2), 75 % (30 mm^2) or 100 % (40 mm^2) of hybridization surface coverage, respectively. A positive linear relationship exists between the heat transfer resistance effect size upon denaturation and the total amount of hybridized DNA ('DNA_{hybr}' expressed as the hybridization surface coverage in mm^2) (ΔR_{th} = 3.15 + 0.38 DNA_{hybr}; R^2 = 0.98), as is illustrated in **Figure 7.** This relationship allows for quantification of a DNA fragment of interest, based on its change in R_{th} upon denaturation. The identified relationship indicates a minimal increase in heat transfer resistance upon temperature ramping, even when no DNA is hybridized to the NCD sample surface. This is in contrast to previously published results showing a nearly constant heat transfer resistance (ΔR_{th} = ± 0) for 0 % hybridization surface coverage [13]. Since the change in R_{th} upon temperature ramping is caused by the denaturation of dsDNA to ssDNA at elevated temperatures, the absence of dsDNA (as is the case for 0 % hybridization surface coverage) would indeed result in a constant heat transfer resistance during temperature ramping. Probably, the heat transfer resistivity technique requires a minimal amount of hybridization surface coverage before changes in heat transfer resistance upon denaturation are detected. The detection limitations of the heat transfer resistivity technique might be reduced through optimization of the signal-to-noise ratio in the future. The theoretical take-off ΔR_{th} value implied by **Figure 7**, might be caused by these suspected detection limitations of the heat transfer resistivity technique.

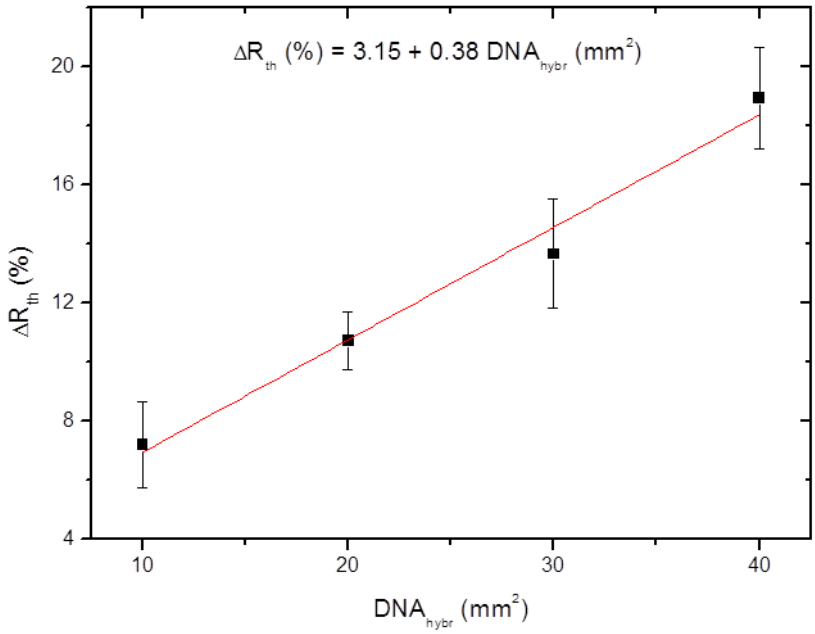

Figure 7: Correlation between heat transfer resistance effect size upon denaturation (ΔR_{th}) and hybridization surface coverage (DNA_{hybr}).

Heat transfer resistance measurements were previously reported to allow for discrimination between SNPs based on differences in denaturation temperature, when both gene polymorphisms were analysed separately [13]. However, up until now, no evidence was presented for the discrimination between two SNPs when both DNA fragments are hybridized to the same NCD sample surface. The results presented in the current study illustrate the possibility to distinguish between a gene fragment and its SNP within the same heat transfer resistance measurement, provided a difference in denaturation temperature exists between both (6 °C in the current study). The heat transfer resistance change effect size upon denaturation caused by the full match DNA fragment on the one hand and the mutated DNA fragment on the other hand shows a similar increase with increased hybridization surface coverage as was observed for the singular detection of the full match gene fragment. This is depicted in **Figure 8** and illustrates the potential to determine the fraction of mutated DNA fragments in a sample of interest. The observed relationship between the hybridized amount of DNA and the heat transfer resistance effect size upon denaturation can be used to evaluate the presence of an aberrant oligonucleotide sequence, even when no sufficient difference in denaturation temperature between a DNA fragment and its nucleotide polymorphism exists. This by comparing the heat transfer resistance effect size upon denaturation after hybridization in low stringent conditions, as performed in the current study, and after hybridization in high stringent conditions. High stringent hybridization can be realized by increasing the washing temperature [19] and/or by adding formamide to the washing solution [20]. High stringent conditions should only allow for hybridization of fully matching oligonucleotide sequences, while in low stringent conditions both the fully matching sequences and the sequence polymorphisms will remain hybridized. This will result in a higher heat transfer resistance effect size upon denaturation for low stringently hybridized NCD-samples as compared to high stringently hybridized NCD-samples, when a sequence polymorphism of the gene of interest is present. Although these results show that differentiation between gene sequence polymorphisms hybridized to the same NCD sample is possible with the heat transfer resistivity technique, successful analysis of mixtures of sequence

polymorphisms also requires simultaneous hybridization of a mixture of different sequence polymorphisms on the same NCD sample. However, based on the theoretical higher stability of the hybridization product of the probe with the fully matching sequence as compared to the hybridization product of the probe with the nucleotide polymorphism [21], the fully matching sequence might be preferentially hybridized when in competition with mutated DNA fragments. This would interfere with the detection of low copy number SNPs. Therefore, in a next step, the heat transfer effect size upon denaturation of NCD samples hybridized with oligonucleotide solutions containing both the full matching oligonucleotide and its SNP in known ratios should be evaluated and compared with correlations between hybridization surface coverage and heat transfer effect size observed in the current study.

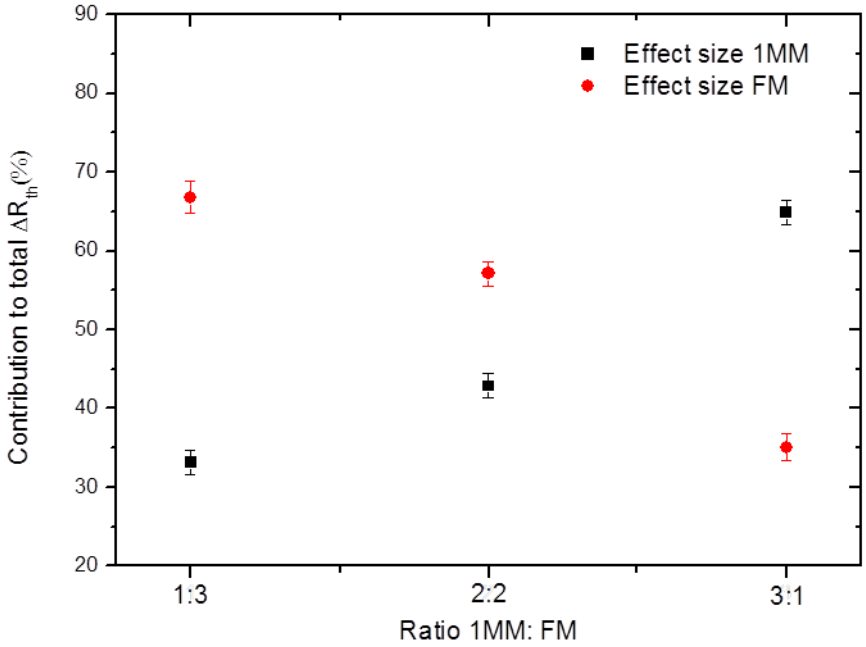

Figure 8: Percentile contributions to the total heat transfer resistance effect size upon denaturation of the mutated sequence fragments (1MM) on the one hand and the fully complementary sequence fragments (FM) on the other hand, observed for heat transfer resistance analysis for different ratios of FM and 1MM DNA hybridized to the same NCD sample (1:3, 2:2, 3:1).

3.6 Conclusions

This study showed the possibility to use the recently developed heat transfer resistivity procedure to determine the gene copy number of a specific gene of interest for the first time. Furthermore, it was proven that the heat transfer resistivity procedure allows for differentiation between DNA fragments representing different sequence polymorphisms of the same gene when analysed simultaneously. This illustrates the potential of this technique as a user-friendly alternative for currently widely used micro-arrays. Moreover, the procedure allows to estimate the mutated fraction of the gene of interest through simultaneous heat transfer resistance analysis of both sequence polymorphisms. Therefore, these results present the heat transfer resistivity procedure as a technique with great potential for implementation in diagnostic procedures in any field of research ranging from clinical diagnostics, environmental microbiology and microbial ecology to detect mutations or polymorphisms. In the future it can allow for the development of a fast and low effort, label-free biosensor to detect gene sequence polymorphism based hereditary diseases such as Alzheimer's disease [22], phenylketonuria [23] and specific types of cancer [24]. Alternatively, a biosensor to distinguish between closely related target and non-target organisms, based on 16S rRNA gene sequence polymorphisms, can be developed with this technique. Such a sensor would be widely applicable to detect human pathogens in patients [25, 26], food industry [27] and drinking water production, to identify plant pathogens in agriculture [28] or to detect bacterial contaminants during food production [29].

3.7 Acknowledgements

Financial support by the Life-Science Initiative of the Province of Limburg, the Research Foundation Flanders FWO (Project G.0829.09: 'Synthetic diamond films as platform material for novel DNA sensors with electronic detection principles') and the EU FP7 through Marie Curie ITN "MATCON" (PITN-GA-2009-238201) is greatly appreciated.

3.8 References

[1] Wenmackers, S, et al., *Phys. Status Solidi A*, 2009, **206**, 391-408.

[2] Vermeeren, V, et al., *Langmuir*, 2008, **24**, 9125-9134.

[3] Christiaens, P, et al., *Biosens. Bioelectron*, 2006, **22**, 170-177.

[4] Yang, W, et al., *Nat. Mater*, 2002, **1**, 253-257.

[5] Krátká, M, et al., *Sens. Actuators B Chem*, 2012, **166-167**, 239-245.

[6] Ingebrandt, S, et al., *Biosens. Bioelectron*, 2007, **22**, 2834-2840.

[7] Poghossian, A, et al., *Biosens. Bioelectron*, 2007, **22**, 2100-2107.

[8] Vagin, M, Karyakin, A,Hianik, T, *Bioelectrochemistry*, 2002, **56**, 91-93.

[9] Poghossian, A, et al., *Sens. Actuators B Chem*, 2006, **118**, 163-170.

[10] Grieten, L, et al., *Physica Status Solidi A*, 2011, **208**, 2093-2098.

[11] Yeap, W, Tan, Y, Loh, K, *Anal. Chem*, 2008, **80**, 4659-4665.

[12] Wang, X, et al., *ACS Appl. Mater. Interfaces*, 2012, **4**, 3526-3534.

[13] Van Grinsven, B, et al., *ACS Nano*, 2012, **6**, 2712-2721.

[14] Janssens, S, et al., *Journal of Chemical Physics*, 2012, **137**, 044702.

[15] Wenmackers, S, et al., *Langmuir*, 2008, **24**, 7269-7277.

[16] Christensen, A, Chang-Yen, D, Gale, B, *J. Micromech. Microeng*, 2005, **15**, 928–934.

[17] Guo, X, et al., *Nature Nanotechnology*, 2008, **3**, 163–167.

[18] Lenz, M, Striedl, G, Fröhler, U, *Infineon Technologies AG*, 2000

[19] Urakawa, H, et al., *Appl. Environ. Microbiol*, 2003, **69**, 2848-2856.

[20] Guan, B, et al., *J. Integr. Plant Biol*, 2008, **50**, 345-351.

[21] Tibanyenda, N, et al., *European Journal of Biochemistry*, 1984, **139**, 19-27.

[22] Martin, E, et al., *Am. J. Hum. Genet*, 2000, **67**, 383–394.

[23] Guldberg, P, et al., *Am. J. Hum. Genet*, 1998, **63**, 71–79.

[24] Dunning, A, et al., *Cancer Epidemiol. Biomarkers Prev*, 1999, **8**, 843–854.

[25] Harald, P, et al., *J. Clin. Microbiol*, 2012, **50**, 3990-3997.

[26] Den Bakker, H, et al., *Appl. Environ. Microbiol*, 2011, **77**, 8648-8655.

[27] Ducey, T, et al., *Appl. Environ. Microbiol*, 2007, **73**, 133-147.

[28] Lievens, B, et al., *FEMS Microbiol. Lett*, 2006, **255**, 129-139.

[29] Justé, A, et al., *Food Anal. Methods*, 2011, **4**, 173-185.

Chapter 4

Optimizing the thermal read-out technique for MIP-based biomimetic sensors: towards nanomolar detection limits

Sensors, 2013, **Submitted**

Bram Geerets[1], Marloes Peeters[1,2*], Bart van Grinsven[1,2], Karolien Bers[1,2], Ward De Ceuninck[1,2] and Patrick Wagner[1,2]

1) Hasselt University, Institute for Materials Research, Wetenschapspark 1, B-3590 Diepenbeek, Belgium
2) IMEC vzw – Division IMOMEC, Wetenschapspark 1, B-3590 Diepenbeek, Belgium

4.1 Abstract

In previous work, the novel heat-transfer method (HTM) for the detection of small molecules with Molecularly Imprinted Polymers (MIP)-type receptors was presented. In this study we focus on optimization of this sensor performance, with as final aim to lower the detection limit by reducing the noise level. It was determined that the noise foremost originates from the power supply, which can be controlled by varying the PID parameters. Therefore, the effect of the individual parameters was evaluated by tuning P, I and D separately at a temperature of 37 °C, giving a first indication of the optimal configuration. Next, a temperature profile was programmed and the standard deviation of the heat-transfer resistance over the entire regime was studied for a set of parameters. The optimal configuration, P1-I6-D0, reduced the noise level with nearly a factor of three compared to the original parameters of P10-I5-D0. With the optimized settings, the detection of L-nicotine in buffer solutions was studied and the detection limit improved significantly from 100 nM to 35 nM. Summarizing, optimization of the PID parameters and thereby improving the detection limit is a key parameter for first applications of the HTM-method for MIP receptors in analytical research.

4.2 Introduction

Molecularly Imprinted Polymers (MIPs) are synthetic materials which mimic the recognition and binding behavior of natural antibodies [1-3]. These tailor-made receptors are highly selective, stable, and resistant to a wide range of pH, solvents and temperature [4, 5]. In comparison to natural receptors, MIPs are cheap due to their straightforward synthesis [6]. These properties make them an interesting tool for different application areas, including separation science and purification [7], biosensors [8], catalysis and drug delivery [9, 10]. For chromatographic purposes, MIPs can be readily used by packing them directly into separation columns [7]. However, the integration of MIPs into sensing devices remains challenging. The majority of the sensor platforms is based on gravimetric detection [11-14] and electrochemical techniques [15-19]. Gravimetric detection is laborious, while the analysis with electrochemical techniques is often complicated. Van Grinsven *et al*. proposed a technique based on heat-transfer resistance to detect single nucleotide polymorphisms in DNA [20]. Recently, a similar approach was employed for signaling molecules with MIP-type receptors [21]. This heat-transfer method (HTM) requires only two thermocouples, a proportional-integral-derivative (PID) controller and an adjustable heat source, eliminating the need of sophisticated equipment. For proof-of-principle purposes, the response of a MIP to increasing L-nicotine concentrations in buffer solutions was studied and a detection limit of 100 nM in buffer solutions was achieved. This is comparable to electrochemical impedance spectroscopy which was used as reference technique. A schematic design of this setup is shown in Figure 1.

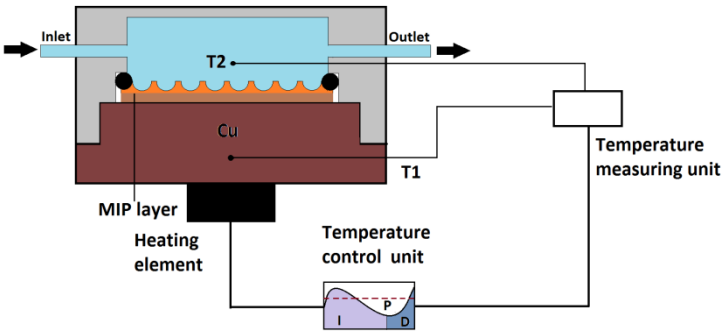

Figure 1: shows schematically the experimental setup. The temperature of the copper block (T_1) is actively steered *via* the temperature control unit through the heating element while T_2, the temperature of the fluid, is solely monitored. For the measurements the power is also a significant factor, which is controlled by the PID-element [14].

In this manuscript we will focus on optimization of the sensor performance, with the aim to lower the detection limit. To this end, the noise level should be reduced since the detection limit corresponds to where the signal is three times the standard deviation. In order to control the temperature of the copper block, an algorithm is combined with a feedback loop. This algorithm functions as a set point controller. The controller implements the proportional value as the present error, where the integral and derivative correspond to the average of the past errors and the prediction of future errors respectively [22, 23]. The effect of the temperature and the PID parameters of the control unit on the noise level are analyzed. As a starting point, the parameters of previous research (P=10, I=5, D=0) are used [20, 21]. These parameters are selected since they ensure high temperature control, with a minimal uncertainty of 0.02 °C from the set temperature. However, for the measurements not solely the temperature is studied, but the heat-transfer resistance which also involves the power. The observed noise in the experiments is mainly due to changes in the voltage, necessary to keep the temperature of the copper

constant. In this manuscript other PID parameters are tested systematically and evaluated if they allow a better tradeoff in temperature and power control, resulting in a lower noise ratio of the overall heat-transfer resistance. Using the optimized PID parameters, the noise level is shown to reduce nearly threefold, lowering the detection limit to 35 nM**.** This is well within the physiologically relevant range of L-nicotine, since salivary and urinary concentrations nicotine are in the micromolar regime, 0.2 – 1000 µM in saliva and 0.3 – 10 µM in urine [24, 25]. Therefore, there is no direct need to further optimize the sensor performance for the detection of this template. However, it should be considered that this read-out technique can also be employed for other targets that are of higher interest for biomedical research, , for instance histamine and serotonin. Horemans *et al.* documented the presence of histamine in blood to be in a range of 10 – 1000 nM and in a regime of 200 – 750 nM in urine. Peeters *et al.* discovered a presence of 10 – 1500 nM of serotonine in blood. These biogenic amines have significantly lower physiologically relevant concentrations in the order of the nanomolar regime. Hereby is demonstrated that optimization of the PID parameters is a key element for future measurements in biological samples [26, 27]. Summarizing, the HTM method enables fast and low-cost measurements and optimizing the sensor performance is an important step for real analytical applications.

4.3 Experimental Section

4.3.1 Design of the sensor setup

In Figure 1 the sensor platform is presented. The MIP substrates are mounted horizontally into a home-made Perspex flow cell with an internal volume of 110 µl. The sensor surface is sealed off from the external environment using an O-ring with an area of 28 mm^2. The substrate was attached to the copper block with silver paste, ensuring good thermal contact. On top of the copper block, the power resistor (MHP TO-220, 20 W, Farnell, Belgium) with a prefixed resistance of 22 Ω, is attached which is connected to the temperature control unit, enabling control of the copper temperature. In order to deliver a specific output voltage to our power resistor, a proportional integral derivative (PID) controller is utilized. This control unit will calculate the necessary output voltage to approach the determined temperature set point. Therefore, two miniaturized thermocouples (Type K, 500 µm, TC Direct, The Netherlands) are used to obtain, respectively, the copper (T_1) and temperature in the fluid (T_2). The first thermocouple (T_1) is placed 4 mm inside the copper block, while the second thermocouple (T_2) is positioned in the flow cell 1.7 mm above the sensor surface in the liquid. The measured temperatures are dispatched to a data acquisition unit (Picolog, TC08, Picotech, United Kingdom) and forwarded to the PID controller. The PID controller compares the prefixed temperature set point and the actual measured temperature and subsequently determines the output voltage towards the power resistor. The output voltage is directed through a second controller (NI USB 9263, National Instruments, USA) to a power operational amplifier (LM675, Farnell, Belgium), before arriving at the power resistor. The setup is equipped with a tubing system which makes it possible to connect it to a programmable syringe pumping system (ProSense, Ne-500, The Netherlands). Additionally, the flow cell contains a gold wire which can be employed as an electrode for impedance measurements [20, 28].

4.3.2 Optimizing the PID settings

The measurements to study the PID settings are performed on a blank aluminum substrate with an area of 1 cm^2 and a flow cell filled with 1× phosphate buffered saline (PBS). The temperature dependence of the PID parameters is evaluated and the optimal settings are determined by analyzing the standard deviation on the signal. The parameters settings with the lowest standard deviation are marked as the optimal configuration. A temperature profile is programmed which consists of, respectively, plateaus and ramps and is in the temperature range of 35 – 85 °C at an ambient temperature of 19.00 °C. The temperature plateaus last 20 minutes, after which the temperature is raised in a controlled fashion with 1 °C/min for 5 min to reach the next plateau. The time in which the temperature is increased will be referred to as the ramping phase. The R_{th} is calculated by dividing the difference in temperature between the copper (T_1) and the fluid (T_2) by the power needed to keep the copper at a constant temperature (Equation 1). The power is obtained by dividing the square of the output voltage by the resistance of the power resistor [20].

$$(1) \quad R_{th} = \frac{T_1 - T_2}{P}$$

The standard deviation on the R_{th} signal was calculated for the plateaus and the ramping phase. For the ramping phase, the R_{th} signal is fitted with a linear fit. Subsequently, this linear fit is subtracted from the R_{th} signal, thereby creating an artificially plateau out of a ramping phase. The standard deviation of this section was calculated over 300 points.

4.3.3 Preparation of the MIP electrode

The synthesis procedure for the MIP and its reference, the non-imprinted polymer (NIP) for L-nicotine are described in detail in ref [8]. To prepare the functionalized electrodes, 1 x 1 cm^2 aluminum electrodes are spincoated with conductive OC_1C_{10}-PolyPhenyleneVinylene (PPV). This PPV derivative, serving as an adhesive layer, is synthesized via the sulfinyl precursor route [29]. MIP and NIP particles are applied to the surface with a polydimethylsiloxane (PDMS) stamp. Subsequently, the layer is heated to 120 °C, allowing the powder to partially sink into the MDMO-PPV layer. After cooling the substrates are washed with isopropanol, ensuring a strong fixation into the layer. The substrates are attached to the copper block, which is kept constant at 37.00 ± 0.02 °C. After stabilizing in 1x PBS, the electrodes are exposed to increasing concentrations of L-nicotine (10 – 1000 nM) in order to determine the detection limit of the sensor platform.

4.4 Results and Discussion

4.4.1 Optimization of the sensor setup

The blank aluminum substrates are mounted into the Perspex flow cell filled with 1× PBS. In order to study the temperature dependence of the PID settings, a temperature profile was designed in a regime of 35 – 85 °C containing intermediate stages every 5 °C. This is shown in Figure 2. The black curve represents the temperature of T_1, the red line demonstrates T_2, and the blue curve stands for the applied power necessary for maintaining the copper temperature at each plateau. The PID settings to compute the representing figure were P5-I8-D0.

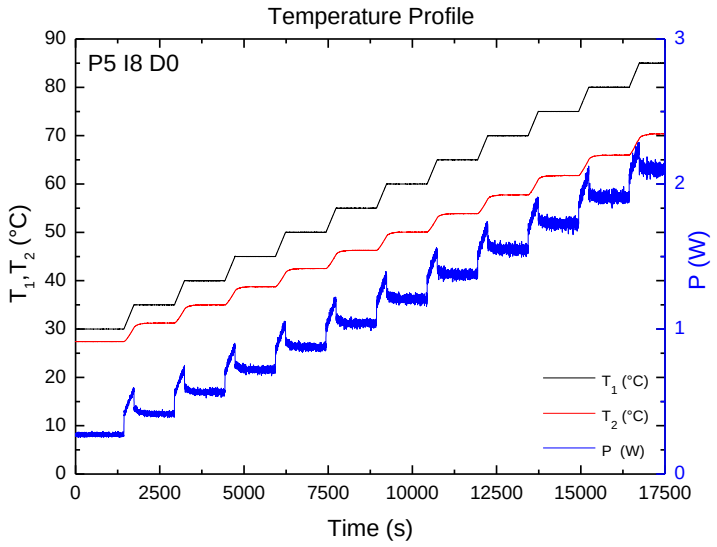

Figure 2: The temperature profile, used to study the noise level, consists of the copper temperature, T_1, (black), the fluid temperature, T_2, (red) and the power applied to the heating element (blue). The profile comprises plateau phases and ramping phases and is presented with a PID configuration of P5-I8-D0.

In order to determine the origin of the noise, foremost the temperature signal was evaluated. The noise of the temperature signal was determined to be 0.02 °C for the entire temperature range (30 – 85 °C). Simultaneously, the power signal was examined where something striking was observed. There was a considerable amount of noise on the power signal, though this was absent in the temperature signal. Hereby, a first indication for optimization of the measuring signal was reflected and it is feasible to optimize the system by reducing the noise of the power supply.

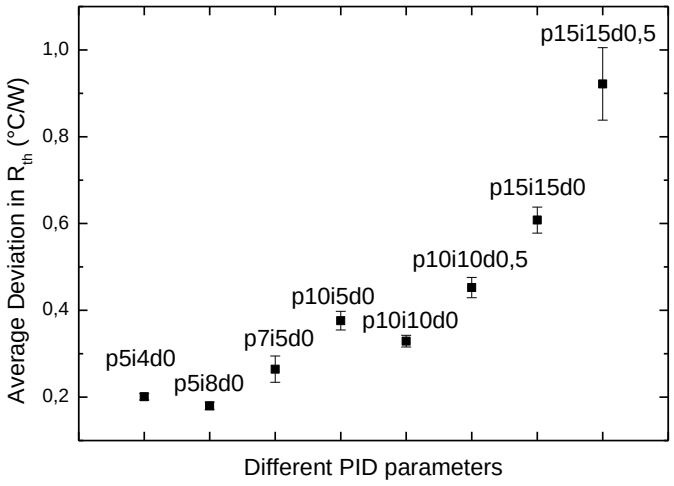

Figure 3: Ten different PID-parameters were examined in a wide regime of configurations at a stable temperature of 37.00 ± 0.02 °C. The average uncertainty in R_{th} is plotted versus the different PID parameters

Therefore, ten distinct different PID configurations were examined at a stable temperature of 37.00 ± 0.02 °C, which are shown in Figure 3. This enabled us to determine the effect of different values for the PID parameters. For instance, a PID configuration of P15-I15-D0.5 resulted in an average uncertainty in R_{th} of 0.921 ± 0.083 °C/W, where PID parameters of P5-I4-D0 result in an average uncertainty of only 0.201 ± 0.007 °C/W. The results of this first PID related effect implied that by omitting the derivative parameter, the noise level is reduced. Furthermore, lowering the effect of the present error showed a diminished noise level on the power signal. These first implications enabled us to demarcate a specific range of PID configurations in order to examine further noise reduction. These configurations are shown in Table 1. To examine the temperature dependency of the PID settings, the above presented temperature profile was applied for every individual PID configuration.

Table 1: The PID parameters shown in this table were selected after demarcating a specific regime. Hereby, it was possible to sharpen the PID parameters to be used. The first column gives a representation of the used PID configurations. The numbers illustrate respectively the proportional, integral, and derivative factors. The second and third column act as the calculated average uncertainty in R_{th} for plateau phases and ramping phases for the entire temperature range.

	Average uncertainties in R_{th} (°C/W)	
PID configuration	Plateau phases	Ramping phases
1-4-0	0.137 ± 0.073	0.105 ± 0.046
1-6-0	0.095 ± 0.058	0.076 ± 0.026
1-8-0	0.101 ± 0.070	0.085 ± 0.022
1-10-0	0.107 ± 0.056	0.081 ± 0.036
3-4-0	0.130 ± 0.077	0.103 ± 0.038
3-6-0	0.153 ± 0.087	0.120 ± 0.047
3-8-0	0.123 ± 0.063	0.093 ± 0.042
3-10-0	0.111 ± 0.069	0.090 ± 0.030
5-4-0	0.168 ± 0.073	0.121 ± 0.067
5-6-0	0.156 ± 0.070	0.113 ± 0.061
5-8-0	0.165 ± 0.086	0.125 ± 0.056
5-10-0	0.144 ± 0.079	0.112 ± 0.046
5-15-0	0.135 ± 0.075	0.105 ± 0.042
10-5-0	0.698 ± 0.150	0.627 ± 0.097

The PID parameters are displayed in Table 1, giving a clear representation of the effect of each individual parameter. Moreover, we still differentiate between plateau phases and ramping phases. However, the representing numbers are averaged out for the entire temperature range and the error number for one PID configuration is rendered in one number. Hereby, it is possible to consider the effect of making small changes in the ratio of the PID parameters. We noticed that PID settings with low proportionality values only improve the signal-to-noise ratio of the heat transfer resistance signal when integral action occurs in a more dominant role. The derivative term was left out of consideration, due the results of the earlier performed experiment.

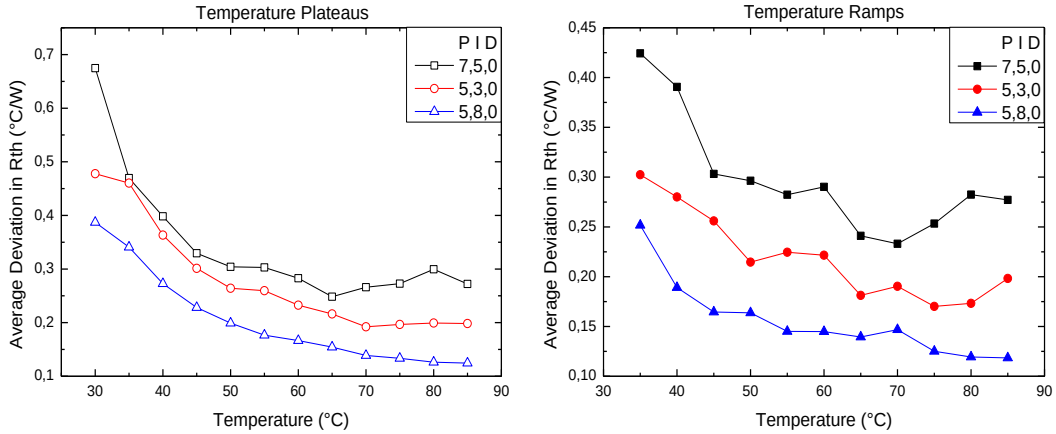

Figure 4: The average uncertainty of the thermal resistance was measured for the entire temperature range. This figure illustrates the average uncertainty in R_{th} for every temperature plateau (A), and temperature ramp (B) for three selected PID configurations. The solid lines are a guide to the eye.

Figures 4A and 4B illustrate the averaged uncertainties of the heat transfer signal at specific temperatures levels for the plateau phases and the ramping phases. Three PID configurations were selected to illustrate the effect of changing the ratio between proportional and integral action. The following PID parameters were used P7-I5-D0, P5-I3-D0, and P5-I8-D0 to give a representative view of the deviation on the thermal resistance signal. As we can see, minor changes in configuration already result in a strong decrease in the average uncertainty of the HTM signal. Table 1 shows that P1-I6-D0 corresponds to the optimal configuration with an average uncertainty of only 0.095 ± 0.058 °C/W for plateau phases and 0.076 ± 0.026 °C/W for ramping phases. In comparison with the prior PID configuration (P10-I5-D0), this results in a 3-fold noise reduction. Furthermore, there is a difference in noise level between plateau and ramping phases. In order to maintain the plateau temperature, the heating element is switched on and off repetitively. This phenomenon results in a more alternating signal. However, due to the optimizing the PID configurations, this effect is minimized. In comparison with the ramping section, here the temperature of the copper is increased at a rate of 1 °C/min. Therefore, the power applied to the heating element is also increasing resulting in less error on the thermal resistance signal. Next to the effect of altering the PID parameters, we also noticed a temperature related effect. At elevated temperatures, the uncertainty of the thermal resistance becomes significantly reduced. The diminishing effect on the signal by increasing the temperature can be elucidated as an effect of heat transfer from the copper not only to the flow cell, but also towards the environment. At elevated temperatures this effect increases tremendously, resulting in an even more stable signal.

4.4.2 Detection limit

In order to prove the lowering of the detection limit by reducing the noise, the detection of L-nicotine with MIPs was studied. In previous work of M. Peeters *et al.*, this detection limit was calculated to be 100 nM. To provide evidence of the influence of the PID configuration on HTM, concentrations are added in the range of 10 – 1000 nM L-nicotine in PBS. The data of these additions is represented in Figure 5.

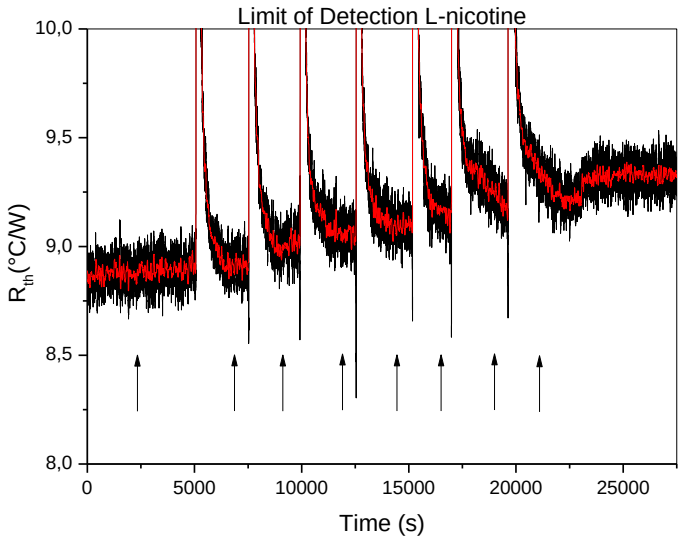

Figure 5: The measurement was performed with the optimized PID parameters of P = 1, I = 8 and D = 0. The Figure shows the response in thermal resistance upon increasing concentrations of L-nicotine (10, 25, 50, 100, 250, 1000 nM). The raw data was filtered with a percentile filter (50%) over 50 points, resulting in the smoothed red line.

The baseline of the R_{th} was stipulated by initiating the measurement in PBS buffer solution, and stabilized at a R_{th} of 8.92 ± 0.04 °C/W. Subsequently, the addition of different concentrations L-nicotine was performed with increasing quantities, comprehending a stabilization period of at least 15 minutes. After each addition, an increase is noticed in R_{th}. The addition of 1 µM L-nicotine resulted in a R_{th} of 9.34 ± 0.06 °C/W, resulting in an effect size of 4.4%. This is significantly higher compared to the size of the noise (0.04%). The difference in R_{th} is calculated by deducting the baseline from the heat-transfer signal for each applied concentration and plotted in a dose-response curve. These results are summarized in Figure 6.

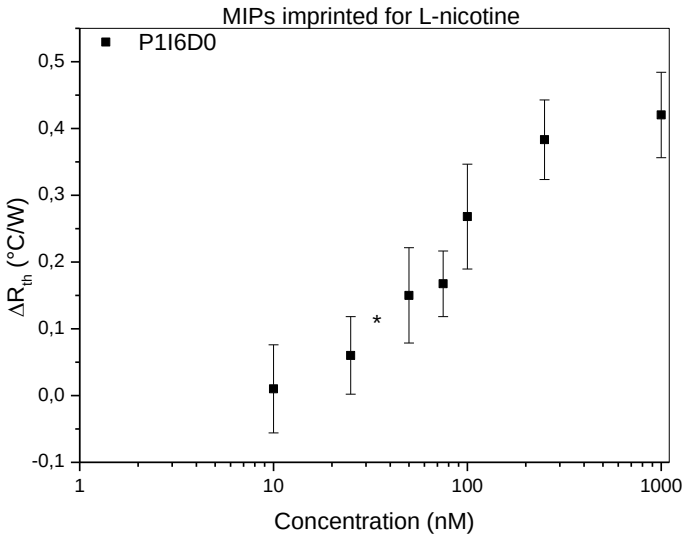

Figure 6: Dose-response curve of the MIP imprinted for L-nicotine. The difference in R_{th} is plotted against logarithmic presented concentration. The concentration of L-nicotine varies in a range from 10 nM to 1 µM. The mathematical detection limit is illustrated by the asterisk.

The dose response curve was constructed for a concentration range of 0 – 1 µM. The standard deviation of the baseline was calculated to be 0.04 °C/W and was used to estimate the detection limit of the electrode, which was set to be three times the standard deviation of the baseline. This resulted in experimental detectable concentrations between 50 nM (ΔR_{th} = 0.15 ± 0,07 °C/W) and 1 µM (ΔR_{th} = 0.42 ± 0.06 °C/W). Additionally, the theoretical detection limit was estimated using a linear fit (R^2 = 0.95) through the dose-response curve. The calculated detection limit was determined to be 35 nM, which lowers it a threefold compared to ref [15].

4.5 Conclusions/Outlook

In this study, we presented the influence of PID parameters on the detection limit for small molecules with MIPs, using HTM as analytical technique. In previous work, Peeters *et al.* showed a detection limit of 100 nM target concentration. These results were obtained with PID parameters of P10-I5-D0, which have a unfavorable high noise level (average uncertainty in R_{th} = 0.698 ± 0.150 °C/W for plateaus and 0.627 ± 0.097 °C/W for ramps). The origin of the noise was located to be in the power signal by separately analyzing the temperature and power data. The applied power is controlled *via* the PID parameters of the PID control unit. The optimal PID configuration, which results in the lowest uncertainty in R_{th}, was calculated in a range from 35 – 85 °C differentiating between temperature plateaus and ramps. This is determined to be P1-I6-D0 (average uncertainty in R_{th} = 0.095 ± 0.058 °C/W for plateaus and 0.076 ± 0.026 °C/W for ramps) reducing the noise level by nearly a factor of three. Subsequently, the detection of small molecules with MIPs was re-examined using the optimized PID parameters. These resulted in a detection limit (35 nM) which is a threefold lower compared to the limit of detection obtained in previous experiments (100 nM). The lowered noise level is required for using HTM for performing measurements in biological samples. Summarizing, the improved signal-to-noise ratio of HTM enables detecting small molecules in the nanomolar range using MIP receptors, which makes it a promising technique for bioanalytical purposes.

4.6 Acknowledgments

This work is supported by the Life-Science Initiative of the Province of Limburg, by the Special Research Funds of Hasselt University, the Methusalem Nano Antwerp – Hasselt, the European Funds for Regional Development – MicroBioMed and the FWO project G.0B62.13N. The authors also would like to thank Prof. T. J. Cleij, H. Penxten, J. Soogen, C. Willems, J. Baccus, L. De Winter, and J. Mertens for technical assistance and stimulating scientific discussions.

4.7 References

[1] Whitcombe, M, Vulfson, E, *Advan. Mat.*, 2001, **13**, 467-478.

[2] Poma, A, Whitcombe, M, Piletsky, S, *Desig. Recep. Next Gen. Biosens.*, 2013, 105-129.

[3] Dickert, F, Lieberzeit, P, Tortschanoff, M, *Sens. Act. B Chem.*, 2000, **65**, 186-189.

[4] Arshady, R, Mosbach, K, *Chem. phys.*, 1981, **182**, 687-692.

[5] Haupt, K, *Chem. Commun.*, 2003, **2**, 171-178.

[6] O'Mahony, J, et al., *Biosens. Bioelectron.*, 2006, **21**, 1383-1392.

[7] Benito-Pena, E, et al., *J. Chromatogr. A.*, 2008, **1208**, 62-70.

[8] Thoelen, R, et al., *Biosens. Bioelectron.*, 2008, **23**, 913-918.

[9] Ye, L, Haupt, K, *Anal Bioanal Chem*, 2004, **378**, 1887-1897.

[10] Sellergren, B, Allender, C, Adv. Drug Deliv. Rev., 2005, **57**, 1733-41.

[11] Reimhult, K, et al., *Biosens. Bioelectron*, 2008, **23**, 1908-1914.

[12] Hayden, O, et al., *Angew Chem Int Edit*, 2006, **45**, 2626-2629.

[13] Dickert, F, et al., *Sens. Act. B: Chem*, 2001, **76**, 295-298.

[14] Dickert, F, Hayden, O, *Trends Anal. Chem.*, 1999, **18**, 192-199.

[15] Piletsky, S, Turner, A, *Electroanalysis*, 2002, **13**, 317-323.

[16] Suryanarayanan, V, Wu, C, Ho, K, *Electroanalysis*, 2010, **22**, 1795-1811.

[17] Peeters, M, et al., *Anal Chem*, 2013, **85**, 1475-1483.

[18] Ramanavicius, A, et al., *Bioelectrochemistry*, 2010, **79,** 11-16.

[19] Ramanavičius, A, et al., A, *Electrochimica Acta*, 2006, **51**, 6025-6037.

[20] Van Grinsven, B, et al., *ACS Nano*, 2012, **6**, 2712-2721.

[21] Peeters, M, et al., *Anal Bioanal Chem*, 2013, (DOI) 10.1007/s00216-013-7024-9

[22] Äström, K, Murray, R, *Feedback systems: introduction for scientists & engineers*, 2008.

[23] Aström, K, *Control System Design*, 2002, 216-251.

[24] Russels, M, et al., *Br Med J*, 1976, **6017**, 1043-1046.

[25] Dome, P, et al., *Neurosci Biobehav Rev*, 2010, **34**, 295-342.

[26] Wymenga, A, et al., *Lancet*, 1999, **353**, 293-294.

[27] Horemans, F, et al., *Sens and Act B. Chem*, 2010, **148**, 392-398.

[28] Van Grinsven, B, et al., *Lab on a Chip*, 2011, **11**, 1656-1663.

[29] Louwet, D, Vanderzande, J, Gelan, A, *Synth Met*, 1995, **69**, 509-510.

Chapter 5

Conclusion and Outlook

In this chapter a summary of the obtained results can be found. It discusses the strengths of the novel techniques discovered in this research, but it also designates matter that is still to overcome. Finally, a quick peek into the near future is provided.

The aim of this project was to evolve the HTM to a format not solely applicable for SNP detection in DNA by thermal denaturation. This assists the development of an universal applicable sensor platform.

The instructions at the beginning of this senior practical training were obvious:

i. Provide assistance in the usage of HTM as a detection format for monitoring the capturing of small molecules on an imprinted polymer
ii. Provide assistance in the evolvement of the HTM in thermally denaturing DNA towards a first model of a SNP detection array
iii. Enhance the thermal read-out strategy for SNP detection and lower the detection limit for small molecules using MIPs

In this research a novel read-out strategy was developed for the specific detection of L-nicotine. This was the first time detection of small molecules based on MIP-type receptors in combination with HTM was applied. Upon binding of the L-nicotine on the sensor surface an increase in R_{th} is noticed. We discovered the ability for detecting small molecules in the nanomolar range (100 nM). These results were validated by employing impedance spectroscopy as a reference test. Furthermore, it is possible to extend this method to other small molecules, histamine and serotonin in buffer solutions. HTM measurements result in a detection limit for these molecules which is in the physiological concentration range. For future implementation of the technique it is wise to investigate the possibility of engaging the MIP sensor surface in combination with the HTM for biological samples. A first experiment was performed for detecting L-nicotine in saliva. The outcome concluded it was possible to monitor the presence of L-nicotine in saliva. However, this only occurred to be a first step in the further development of the MIP-based sensor platform.

The second study was performed on monitoring the thermal denaturation of different DNA sequences simultaneously . First the effect of surface coverage was examined by dividing the NCD sample in four compartments. We were able to differentiate in R_{th} between a hybridized surface coverage of 25 %, 50 %, 75 % and 100 % respectively. A positive linear relationship was noticed between the thermal resistivity of the NCD sample and the increasing the surface coverage. Hereby, we enabled the option for determining the amount of hybridized DNA on the sample surface. In previous studies, the ability of SNP detection was reported. Moreover, this detection was done upon thermal denaturation by monitoring the heat-transfer through the NCD sample. However, the differentiation between healthy and mutated DNA was done by comparing separately performed measurements. In this study we reported about discriminating between complementary and SNP containing DNA fragments hybridized at the same NCD sample. We were able to distinguish between the two different DNA fragments. The contribution to the heat-transfer resistance of both sequences was defined by effect size. Denaturing complementary DNA has a higher impact on the R_{th} compared to its SNP variant. This novel approach allows us to estimate the mutated fraction of the gene of interest and has the potential for implementation in diagnostic procedures.

After developing the two sensor platforms, a closer look at the R_{th} was taken. It was obvious that the signal – to – noise ratio of the signal was not highly favorable. In order to enable the implementation of HTM as read-out strategy in the diagnostic world the signal first needs to be optimized by configuring the PID settings. The average uncertainty of the previous recorded R_{th} was determined to be 0.698 ± 0.150 °C/W for a plateau phases

0.627 ± 0,097 °C/W for a ramping phase. This uncertainty was reduced tremendously. The newly found PID setting were P1-I6-D0 which has an average uncertainty of in R_{th} = 0.095 ± 0.058 °C/W for plateaus and 0.076 ± 0.026 °C/W for ramps reducing the noise level with nearly a factor of three. These settings were implemented in the re-examination of the detection of small molecules providing a lower detection limit for the capturing of L-nicotine (35 nM). The enhanced PID parameters are necessary for measuring biological samples.

The future applicability of HTM as standard read-out strategy is a realistic vision. The HTM based format is a fast and label-free technique and was already employed for the detection of small molecules on a MIP sensor surface and the identification of genes hybridized on a NCD surface. Future pursuits are to extend the number of measurements that rely on HTM. For example to engage HTM for the detection of living cells, lipids and antibody based measurements. At this moment we are already examining the presence of small molecules in biological samples is analyzed by the HTM read-out technique. Moreover, the functionalization of the DNA fragments and its dependency of the NCD substrate is investigated. Hereby we endeavor to design a biosensor that is applicable in bioanalytical industry.

Auteursrechtelijke overeenkomst

Ik/wij verlenen het wereldwijde auteursrecht voor de ingediende eindverhandeling:
Investigating the applicability of heat-transfer resistance as read-out strategy for the detection of mutations in DNA sequences and the detection of neurotransmitters when bound into molecular imprinted polymers

Richting: **master in de biomedische wetenschappen-bio-elektronica en nanotechnologie**
Jaar: **2013**

in alle mogelijke mediaformaten, - bestaande en in de toekomst te ontwikkelen - , aan de Universiteit Hasselt.

Niet tegenstaand deze toekenning van het auteursrecht aan de Universiteit Hasselt behoud ik als auteur het recht om de eindverhandeling, - in zijn geheel of gedeeltelijk -, vrij te reproduceren, (her)publiceren of distribueren zonder de toelating te moeten verkrijgen van de Universiteit Hasselt.

Ik bevestig dat de eindverhandeling mijn origineel werk is, en dat ik het recht heb om de rechten te verlenen die in deze overeenkomst worden beschreven. Ik verklaar tevens dat de eindverhandeling, naar mijn weten, het auteursrecht van anderen niet overtreedt.

Ik verklaar tevens dat ik voor het materiaal in de eindverhandeling dat beschermd wordt door het auteursrecht, de nodige toelatingen heb verkregen zodat ik deze ook aan de Universiteit Hasselt kan overdragen en dat dit duidelijk in de tekst en inhoud van de eindverhandeling werd genotificeerd.

Universiteit Hasselt zal mij als auteur(s) van de eindverhandeling identificeren en zal geen wijzigingen aanbrengen aan de eindverhandeling, uitgezonderd deze toegelaten door deze overeenkomst.

Voor akkoord,

Geerets, Bram